Leaf Microscopy Applications in Photosynthesis Research: Identifying the Gaps

Roxana Khoshravesh[1], Natalie Hoffmann[2], David T. Hanson[1]

[1] Department of Biology, University of New Mexico, Albuquerque, NM, USA

[2] Department of Cell and Systems Biology, University of Toronto, Toronto, ON, Canada

Roxana Khoshravesh: rkhoshravesh@unm.edu

Natalie Hoffmann: natalie.hoffmann@mail.utoronto.ca

David T. Hanson: dthanson@unm.edu

Corresponding author: Roxana Khoshravesh, rkhoshravesh@unm.edu

Highlight

Here, we review the techniques applied in leaf imaging to model anatomy and locate metabolites, as well as evaluate their power and efficiency in addressing fundamental questions in photosynthetic research.

Abstract

Leaf imaging via microscopy has provided critical insights into research on photosynthesis at multiple junctures, from the early understanding of the role of stomata, through elucidating C_4 photosynthesis via Kranz anatomy and chloroplast arrangement in single cells, to detailed explorations of diffusion pathways and light utilization gradients within leaves. In recent decades, the original two-dimensional (2D) explorations have begun to be visualized in three-dimensional (3D) space, revising our understanding of structure-function relationships between internal leaf anatomy and photosynthesis. In particular, advancing new technologies and analyses are providing fresh insight into the relationship between leaf cellular components and improving the ability to model net carbon fixation, water use efficiency, and metabolite turnover rate in leaves. While ground-breaking developments in imaging tools and techniques have expanded our knowledge of leaf 3D structure via high-resolution 3D and time-series images, there is a growing need for more *in vivo* imaging as well as metabolite imaging. However, these advances necessitate further improvement in microscopy sciences to overcome the unique challenges a green leaf poses. In this review, we discuss the available tools, techniques, challenges, and gaps for efficient *in vivo* leaf 3D imaging, as well as innovations to overcome these difficulties.

Keywords: leaf imaging, three-dimensional imaging, metabolite imaging, photosynthesis, microscopy, leaf three-dimensional modeling, leaf anatomy modeling, mesophyll conductance, Raman micro-spectroscopy, infrared spectroscopy, hyperspectral imaging

Introduction

Throughout the history of photosynthetic research, from the early understanding of the role of stomata in leaf gas exchange (Blackman and Darwin, 1895), through the explorations of CO_2 diffusion pathways within intercellular air spaces and across the wet surface of mesophyll cells (Coulter *et al.,* 1910; Turrell, 1936), to elucidating C_4 photosynthesis via Kranz anatomy (Hatch and Slack, 1966) and light utilization gradients within leaves (Allen *et al.,* 1970; McClendon, 1984), leaf form and function research depended on detailed microscopic observations. Some earliest concepts, such as the function of the "*Orifices*" (stomata) on the "skin" (epidermis) to allow leaves to allow the air in and out, date to 1682 by Nehemiah Grew(Grew, 1682) where he explained the function of leaf structures as: "*methods which nature takes to preserve them [leaves] from the injuries both of the ground and of the weather*". But despite this early kick-off, it was not until the 20th century that high-resolution technologies including electron microscopy, laser scanning confocal microscopy, hyperspectral imaging, digital cameras, and sophisticated computational and statistical analyses allowed leaf imaging to become routine in addressing central questions related to photosynthetic form and function.

Here we review the significance of leaf 3D imaging, the implementation of microscopy techniques in photosynthetic research, and their strengths and limitations in keeping up with the demand for high-quality and high-throughput phenotyping. Leaf imaging extends beyond microscopy; however, here we refer to imaging techniques coupled with microscopy. Sensor-based imaging techniques such as hyperspectral remote sensing, thermal infrared, and precision agriculture are reviewed by multiple groups and authors (Li *et al.,* 2014; Adão *et al.,* 2017; Mishra *et al.,* 2017; Nguyen *et al.,* 2020). Furthermore, we discuss the instances where challenges in photosynthesis research would benefit from embracing the current imaging techniques.

1- The Leaf: a 3D dynamic complex

During the evolution of megaphylls in early terrestrial habitats, leaves optimized the arrangement of chloroplasts - the site of CO_2 fixation by Rubisco - within the mesophyll cells and the mesophyll cells within the leaf tissue to maximize photosynthesis (Nicotra *et al.,* 2011; Terashima *et al.,* 2011; Xiao *et al.,* 2016). In addition, within each photosynthetic cell, positioning of mitochondria and peroxisomes along the chloroplasts facilitated (photo)respiration (Sage and Sage, 2009; Baker *et al.,* 2010; Hu *et al.,* 2012; Busch *et al.,* 2013; Hatakeyama and Ueno, 2016), and across a leaf, the venation architecture was coordinated with stomatal position and density to regulate water movement and evaporation (Sack and Holbrook, 2006). These arrangements (Figure 1) create a heterogeneous 3D complex encompassing constant and dynamic paths for light to penetrate to the multiple layers of the leaf; for CO_2 to diffuse from ambient air to the site of carbon fixation; for metabolites to be exported to the other cellular compartments or adjacent tissues such as vascular bundles; and for water to maintain the leaf hydrology (Evans, 1999; Tholen *et al.,* 2012; Li *et al.,* 2017; Earles *et al.,* 2019).

In a mature leaf, the constant path encompasses gross stomatal morphology and density, leaf venation, mesophyll organization, and intercellular airspace (IAS, Figure 1), all of which are established during the leaf development, determined by genetic background (Peterson *et al.,* 2010; Zwieniecki and Boyce, 2014; Chater *et al.,* 2017; Baillie *et al.,* 2019; Scanlon *et al.,* 2019), and influenced by growing conditions such as light level, temperature, available water, and age. For instance, growing in shade decreases the leaf thickness (Oguchi *et al.,* 2005), increases IAS (Allard *et al.,* 1991; Slaton and Smith, 2002), and alters the rate or dimension of cell division and the ratio of the palisade to spongy tissue (Ivanova and Pyankov, 2002; Terashima and Yano, 2004; Kalve *et al.,* 2014; Wu *et al.,* 2017). Growing in high temperatures induces lower stomatal density (Crawford *et al.,* 2012), and growing under and above the optimal temperatures compromises cell division and leaf growth (Rymen *et al.,* 2007; Gray and Brady, 2016). During leaf development, local and uneven

deposition of the primary cell wall establishes mesophyll shape and geometry necessary for the 3D structure of the mesophyll tissue (Panteris and Galatis, 2005; Ambrose *et al.,* 2013; Giannoutsou *et al.,* 2013; Sotiriou *et al.,* 2015). Changing the structure and thickness of the cell wall, either during stress conditions (Roig-Oliver *et al.,* 2020; Warming, 2020), through mutation of cell wall biosynthetic genes (Weraduwage *et al.,* 2016; Ellsworth *et al.,* 2018; Danila *et al.,* 2021), or aging (Hanba *et al.,* 2001; Marchi *et al.,* 2008; Tosens *et al.,* 2012*a*; Clarke *et al.,* 2021) can impact cell size and shape, thus impacting 3D leaf architecture, or modify the access of photosynthetic cells to CO_2 due to changes in thickness and chemical composition of the cell wall.

The dynamic path consists of the stomatal aperture response to light and CO_2 (Engineer *et al.,* 2016); cell wall dynamic metabolism and antioxidant state (Clemente-Moreno *et al.,* 2019), cell membrane, cytosol, and organelles dynamics (Evans *et al.,* 2009; Evans, 2020); and biochemistry (Figure 1). This path is also regulated by genetic background and growing conditions. For example, the arrangement and ultrastructure of chloroplasts vary between C_3 and C_4 species and within C_4 species of different biochemical subtypes (Fisher and Ray, 1982; Edwards and Voznesenskaya, 2011; Stata *et al.,* 2014), within different cell layers of a C_3 leaf (Terashima and Inoue, 1984, 1985), or within species grown in different environments (Taylor and Craig, 1971; Jiang *et al.,* 2011). Besides, well-established evidence confirms chloroplast photorelocation to prevent photodamage or provide access to more light (Kasahara *et al.,* 2002; Suetsugu and Wada, 2005; Wilson and Ruban, 2020); as well as the response of mitochondria, the nucleus, and cytoskeleton to the fluctuating environmental light (Islam *et al.,* 2009; Higa *et al.,* 2014; Perico and Sparkes, 2018; Fujii *et al.,* 2020).

These examples represent the immense diversity in leaf structure between species, within the species grown in different environments, and within cellular layers of a single leaf. The magnitude of this diversity and its effect on photosynthetic capacity have provoked researchers to recognize and implement the intricacy and diversity of the leaf 3D structure in dynamic processes such as leaf internal CO_2 diffusion and mesophyll and stomatal conductance (Turrell, 1936; Nobel,

1977; Longstreth *et al.,* 1980; Nobel and Hartsock, 1981; Thain, 1983; Evans *et al.,* 1994; Théroux-Rancourt *et al.,* 2017; Earles *et al.,* 2018; Lundgren *et al.,* 2019; Xie *et al.,* 2021). International efforts for crop improvement call for leaf anatomy modification as a promising approach for improving the efficiency of photosynthesis (Niinemets *et al.,* 2009; Covshoff and Hibberd, 2012; Tholen *et al.,* 2012; Leegood, 2013; Ren *et al.,* 2019; Lundgren and Fleming, 2020). However, data are not readily available for models to incorporate structural dynamics of the crop beyond generally known leaf traits, or to include rapid responses of organelles to the environmental conditions and the metabolite turnover between leaf sub-compartments.

Current methods rely on simplifications that disregard the depth of the tissue and the dynamics of leaf metabolism over time or dismiss the extent of leaf structural diversity. A remarkable example is the Kranz anatomy of C_4 species. Since its discovery (Hatch and Slack, 1966), plant physiologists -inferring from 2D leaf cross-sections - believed that C_4 species have enlarged bundle sheath cells relative to their C_3 species. However, imaging C_4 leaves from a parademal view revealed that the modification in the direction of expansion, not the bundle sheath size, creates the erroneous perception of larger bundle sheath in C_4 species (Danila *et al.,* 2018; Khoshravesh *et al.,* 2020). Although available microscopy techniques can correct these types of misconceptions, our incomplete understanding of the leaf 3D structure is mainly limited by the development and accessibility of visualization and imaging tools.

Plant leaves are heterogeneous organs consisting of many cell layers of variable sizes, with differences in cell wall thickness, organelle density, and vacuole size. This assortment plus the presence of numerous auto-fluorescing chloroplasts and IAS complicates optical properties in cellular and subcellular levels. Spaced by IAS, leaf cells are also very large - up to 1,280 μm^3 in rice and 12,500 μm^3 in wheat mesophylls (Harwood *et al.,* 2020); therefore, the gas and metabolites moving inside the leaf cell layers travel through biophysically similar long distances and biophysically diverse short distances, passing through approximately 10 nm membranes (Sandelius *et al.,* 1986) or

the ~2 µm width of a mitochondrion (Figure 1); all these paths significantly impact the photosynthetic activities (Evans *et al.,* 1994; Evans and Von Caemmerer, 1996; Evans, 2020). The methods capable of imaging large areas or volumes lack resolution depths to resolve small objects, while instruments efficient in capturing high resolution do not cover a large area or volume. Besides, the rapid response of the dynamic path to the fluctuating environment and fast metabolite movement within and between cells demands 3D leaf imaging capable of collecting fast and efficient time series. This complexity may explain why, despite its significance, there has been approximately twice as much 3D cell imaging research on comparatively simple-structured root cells relative to leaf cells (Figure 2). While considerable progress in imaging techniques has improved our overall knowledge of leaf 3D structure with a rapid rise in recent publications on leaf 3D anatomy (Figure 2), there are many gaps to fill and more to anticipate from future innovations, particularly in the field of *in vivo* and metabolite imaging.

2- Green leaves: commonly applied imaging techniques and challenges

Bright-field light microscopes provided the first insights into leaf anatomy (Grew, 1682; Baillon, 1882) and have been instrumental in outlining fundamental concepts (Table 1). The initial contrast and resolution restriction of bright-field light microscopes have been enhanced by tissue preparation (thin sectioning and staining) and complementary illumination methods (darkfield, phase-contrast, and differential interference contrast or DIC, Table 1) up to its inherent diffraction limit of visible light (200 nm) known as the Abbe limit (Stelzer, 2002). Conventional light microscopes cannot distinguish objects closer than ½ wavelength of visible light (400-700 nm). Thus, for the resolutions higher than 200 nm (1/2 of the blue light wavelength), light microscopes were traditionally supplemented by transmission electron microscopy (TEM), which can detect subcellular details to 0.2 nm resolution. TEM details became accessible via application of chemicals (Ayache *et al.,* 2012), which ultimately can cause size alteration and introduce artifacts (Michen *et al.,* 2015;

Zhang *et al.,* 2017). Cryo-EM and liquid-cell TEM mitigate some of these issues (Chen and Wen, 2012) by retaining cellular structures in a more native state; but, tissue destruction by sectioning the tissue is still required for TEM-based leaf imaging (Table 1).

Fluorescence-based optical microscopy (Table 1) is another solution to enhance contrast and resolution, and add depth to imaging. Fluorescence-based microscopy relies on either endogenous fluorescence, a fluorescing dye, a fluorophore-conjugated primary or secondary antibody, or fluorescent reporters genetically engineered into the living cell; in all scenarios, the localization of the fluorescing source is identified by its emission wavelength. The wide variety of fluorescent microscopy techniques such as laser scanning confocal, non-linear multiphoton, super-resolution, spinning disk, fluorescence lifetime imaging (FLIM), light-sheet fluorescent microscopy (Table 1), or a combination of them have added depth, dynamics, and resolution (up to a single molecule) to live-cell imaging (Renz, 2013; Ovec *et al.,* 2015; Thorn, 2016).

Green leaves provide opportunities and limitations for fluorescence-based microscopy. The autofluorescence from chlorophylls in the red region and phenolic compounds of cuticles and cell walls in green regions of the visible spectrum provides an excellent opportunity for dye-free imaging (Vogelmann and Evans, 2002; Vermaas *et al.,* 2008; Brodersen and Vogelmann, 2010; Collins *et al.,* 2012; Slattery *et al.,* 2016; Lichtenberg *et al.,* 2017; Borsuk and Brodersen, 2019). The autofluorescence from cuticles and cell walls is generally distinguishable from fluorescent dyes and markers in the green region and could be eliminated by laser scanning confocal microscope or by image processing. However, the number of fluorescent dyes is limited because chlorophyll autofluorescence naturally overlaps with emission wavelength greater than 600 nm, and autofluorescence from highly lignified cell walls such as xylem interferes with the green emission peaking in 530 nm wavelength. As well, most manufactured dyes are optimized for animal and human cells. Therefore, they may not efficiently infiltrate the cells due to the thick cell walls and cuticles or they may have a non-specific binding of the markers and generate signals greater than

the targets, which challenges automated segmentation and computational analyses. Furthermore, leaves are optically dense. When one-photon excitation is performed on the intact leaf, light does not penetrate deep into the leaf due to the higher light absorption and scattering by chloroplasts in upper illuminated cell layers (Jacques, 2013). This limits the whole *in vivo* leaf imaging depth up to 100 µm or shorter (sometimes only to the epidermis). Non-linear (two or multi-photon) excitation (Ryu *et al.,* 2014) and light-sheet fluorescent microscopy techniques (Table 1) can improve imaging depth and speed with less damage to the tissue in live-cell imaging. But despite their powerin 3D and live-imaging of the developing organs such as differentiating flowers, growing roots, and juvenile leaves (Capua and Eshed, 2017; Ovečka *et al.,* 2018; Valuchova *et al.,* 2019, 2020; Mizuta, 2021), light-sheet and multi-photon microscopy have not been widely embraced in mature leaf live imaging. This may be explained by the challenges (autofluorescence, optical density, cellular heterogeneity) that green leaves pose to 3D imaging which also delayed the use of more advanced techniques such as super-resolution microscopy (Ovec *et al.,* 2015; Schubert, 2017).

3- Leaf 3D visualization

Internal leaf anatomy models have been primarily developed to estimate the internal leaf CO_2 diffusion path and the light environment.

CO_2 diffusion path: To be fixed in the form of sugars and carbohydrates, CO_2 diffuses (purple arrows, Figure 1) from the sub-stomatal cavity to the IAS - or gas phase - and through the cell wall and membrane, cytosol and chloroplasts - together known as liquid phase (Evans *et al.,* 1994; Syevertsen *et al.,* 1995). The size and arrangement of IAS, and the ratio of the total surface of mesophyll cells exposed to the IAS (S_m or A_{sm}) to the leaf surface area, as well as mesophyll cell wall thickness, chloroplast thickness, and the surface area of chloroplasts exposed to the IAS impact mesophyll diffusion conductance to CO_2 (g_m) (Coulter *et al.,* 1910; Onoda *et al.,* 2017; Evans, 2020). Models to predict *gm* from these quantitative leaf traits using 2D light and electron micrographs of mesophyll tissue and cellular ultrastructure have created fundamental insight into the role of gas

and liquid phases on the efficiency of CO_2 diffusion into chloroplasts (Turrell, 1936; Nobel, 1977; Longstreth *et al.,* 1980; Nobel and Hartsock, 1981; Thain, 1983; Evans *et al.,* 1994; Tosens *et al.,* 2012*b*; Veromann-Jürgenson *et al.,* 2017; Tosens and Laanisto, 2018). These models predicted *gm* values that deviated from the measured values only by 24 % across a wide variety of species and diversity of leaf anatomies (Tosens and Laanisto, 2018).

Currently, to estimate S_m and IAS volume from leaf anatomy, mathematical modeling and simulations are combined with imaging technologies ranging from conventional light microscopy (Evans *et al.,* 1994; Slaton and Smith, 2002; Tosens *et al.,* 2012*a*,*b*; Tomás *et al.,* 2013) to synchrotron radiation X-ray laminography and Micro-Computed Tomography (micro-CT)-based leaf 3D reconstruction (Ho *et al.,* 2016; Théroux-Rancourt *et al.,* 2017, 2020; Earles *et al.,* 2018; Lundgren *et al.,* 2019; Piovesan *et al.,* 2021). While synchrotron radiation-based spectroscopy and micro-CT estimate the most accurate S_m based on the real 3D reconstruction of the intact leaves, our fundamental knowledge on the contribution of S_m and IAS volume to g_m emanate from light microscopy images of the cross, paradermal, and oblique sections from resin- or paraffin-embedded leaf blocks plus models estimating S_m from 2D images (Turrell, 1936; Thain, 1983; Evans *et al.,* 1994; Slaton and Smith, 2002). Comparing four 2D models to estimate S_m, Théroux-Rancourt *et al.* (2017) showed that Turrell's cross and paradermal section model (Turrell, 1936) produced the most accurate S_m values closest to the 3D estimation - within 10% of the 3D median. However, this accuracy requires more sections relative to the methods such as curvature correction factor (Thain, 1983); and eliminating the leaf sections that contain vasculature demands even more sections for the species with denser reticulate venation such as sunflower.

Sample preparation and microtome sectioning to acquire acceptable replicates and slice numbers to estimate S_m and IAS volume are labor-intensive and time-consuming. Each resin block requires at least 3-5 days of chemical infiltration and resin embedding; a few hours of sectioning, staining, and imaging; and few hours of quantification. This restricts the scale of experiments usually

to a few species and replicates in each research project. Moreover, leaves shrink during sample preparation, resulting in error in S_m and IAS estimation; the error being greater in thick (400 µm) relative to thin (100 µm) leaves (Théroux-Rancourt *et al.,* 2017). In contrast, sample preparation is minimal for micro-CT imaging and imaging is fast; up to 50 mm^2 fresh leaf cuts with a depth of 1 mm could be scanned in 30 min to generate thousands of scans (Earles *et al.,* 2019; Lundgren *et al.,* 2019). However, the analysis of these massive datasets is computationally intensive and usually, the segmentation processes reduce the speed, accuracy, and reproducibility of data analysis. Recently, the machine-learning-based segmentation and quantification model (Théroux-Rancourt *et al.,* 2020) enabled model training with a minimum of six scans in less than 30 min, and analysis of more than 1500 micro-CT scans in few hours with more than 90 % accuracy. But, not many researchers have access to micro-CT technology or are capable of conducting computationally intensive data analyses. To fill the gap between the time- and labor-demanding leaf microtome sectioning and the expensive and infrequently accessible micro-CT, techniques such as tissue optical clearing (TOC) could reconstruct 3D leaves for S_m and IAS quantification (Box 1; Figure 3).

In estimating S_m and IAS, one significant limitation is the small imaged/scanned area or volume – up to 4 mm^2 5 mm^2 x leaf thickness with micro-CT, which does not represent the structure of the whole leaf. Although, we know which 2D method provides the least error relative to the 3D techniques (Théroux-Rancourt *et al.,* 2017), both approaches rely on removing veins and focusing on homogenous leaf parts which could introduce the same bias in measurements. We still do not know whether analyzing larger area/volume at the expense of lateral and axial resolution would add more accuracy in understanding leaf features or will introduce more error, and in either case, how much area/volume from how many leaves would represent leaf features accurately. Another limitation is that the areas or volumes imaged during IAS and S_m estimation are not efficient in identifying the critical details of the liquid phase diffusion paths - mesophyll cell wall thickness, chloroplast thickness, and the surface area of chloroplasts exposed to the IAS - on which net photosynthesis also depends (Evans *et al.,* 2009; Evans, 2020). In C_3 species, the access of each

mesophyll chloroplast to CO_2 and O_2 varies based on its proximity to the cell wall facing intercellular airspaces, and cytosol thickness (Evans *et al.,* 1994; Tomás *et al.,* 2013; Veromann-Jürgenson *et al.,* 2020; Clarke *et al.,* 2021). Net photosynthesis is also influenced by the density and position of mitochondria which release photorespiratory CO_2 in the leaf (Sage and Sage, 2009; Busch *et al.,* 2013). Since chloroplasts are the final destination of light and CO_2, the optimized arrangement of the 3D structure of stroma and grana thylakoids, where photosystems (PSI and PSII) and light-harvesting systems are located, and stroma, where Rubisco is localized, is necessary to maximize efficient delivery of light and CO_2 to their final destination (Kirchhoff, 2019).

Some of the closest-to-ideal leaf 3D reconstructions that cover a large cube of the leaf (100 µm x 100 µm x leaf thickness) while maintaining the structural details up to a resolution of 0.75 µm have been created by synchrotron X-ray computed micro-laminography (Verboven *et al.,* 2015; Ho *et al.,* 2016). However, this resolution is insufficient to model 3D CO_2 diffusion and light behavior inside the tomato leaf, so Ho *et al.* (2016) computationally simulated chloroplasts inside mesophyll. To this date, and as reviewed by Earles *et al.* (2019), EM or EM-driven 3D reconstruction methods including SBF-SEM (Serial Block-Face Scanning Electron Microscopy), FIB-SEM (Focused Ion Beam Scanning Electron Microscopy), and TEM tomography (Table 1) have been the sole solution to depict the maximum number of subcellular components in a single frame with the resolution high enough to detect ultrastructural details such as plasmodesmata and membranes (Jin *et al.,* 2018; Yamane *et al.,* 2018), characterize plant cell organelles, and reconstruct chloroplast inner membrane networks (Table 1) (Perktold *et al.,* 1998; Austin and Staehelin, 2011; Daum and Kühlbrandt, 2011; Engel *et al.,* 2015; Kirchhoff, 2019; Wang *et al.,* 2019).

EM-based 3D reconstruction requires post-processing segmentation which has largely relied on manual tracing of the organelles and subcellular boundaries. This could reduce time efficiency, constrain automation of image segmentation for data analysis, and introduce human error. Efforts for automatic segmentation of the EM-based images have recently resulted in the development of

machine learning networks that efficiently segmented membrane-bound organelles, *e.g.* Golgi, lysosome, and mitochondrial, and non-membrane-bound structures, *e.g.* ribosomes and microtubules, as well as 3D-reconstructed multiple human cell types at 4 nm voxel resolution FIB-SEM volumes (Heinrich *et al.,* 2021). Further application of such networks using plant cells as training data would increase the power of EM-based techniques in the subcellular 3D reconstruction of plant cells. However, with all the power and resolution, EM-driven 3D imaging is not accessible for many researchers, leaving them with traditional 2D TEM imaging.

Another leaf 3D modeling approach is simulations using a combination of empirical data with the assumption of regular geometric cellular structure – *e.g.* cylinder-like palisade, sphere-like mesophyll cells, and regular distribution of IAS (Govaerts *et al.,* 1996; Jacquemoud and Frangi, 1997; Ustin *et al.,* 2001; Aalto and Juurola, 2002; Xiao *et al.,* 2016). In these works, the irregularity of the mesophyll surface and the non-homogenous porosity of the leaf have been acknowledged; yet, lacking fast and proper tools to capture its details prevented this irregularity to be applied in the models. The regular geometric simulations have usually represented a "typical C_3 eudicot broadleaf" with one layer of palisade mesophyll and few layers of spongy cells (Ustin *et al.,* 2001; Aalto and Juurola, 2002; Xiao *et al.,* 2016). These models do not cover many of the diverse features of leaves, such as leaves with more than one palisade layer, hypodermis, and multilayered epidermis; succulent leaves with 3D leaf venation and water storage cells (Ogburn and Edwards, 2013); floating aquatic leaves with no palisade (Kaul, 1976); C_3 monocots including diverse groups of grasses, orchids, and Bromeliads; the specialized anatomy of CAM plants (Nelson and Sage, 2008); and C_2 and C_4 species with varying proportion of mesophyll and vascular tissue (Sage *et al.,* 2014; Lundgren, 2020). Within the category of the typical C_3 eudicot broadleaf, the experimental data represent measurements from very few and sometimes a single species, as in Xiao *et al.* (2016) when the number and size of chloroplasts in mesophyll cells of a C_3 species were inferred from tobacco, despite the vast diversity of the chloroplast size and number in C_3 eudicots (Stata *et al.,* 2014). Using limited information only amplifies the already existing bias in the estimation of anatomical features

in 2D EM images (Harwood *et al.,* 2020). Developing publicly available data repositories to collect numerical leaf anatomy data that are currently scattered over published literature, recording the growing condition during the data collection, as well as creating interactive leaf models would be extremely helpful to feed the simulated leaf models with more realistic measurements.

At the cellular level, another factor that alters g_m is the presence of the plant cell wall - composed of polysaccharides (cellulose, hemicellulose, and pectin), phenolics, ions, and proteins. Numerous studies have observed a negative correlation between cell wall thickness (as assessed through EM images) and g_m in diverse plant species (Tomás *et al.,* 2013; Veromann-Jürgenson *et al.,* 2017; Ren *et al.,* 2019; Sugiura *et al.,* 2020), and recent work has highlighted how changes to the chemical composition or cross-linking of cell wall components could also affect g_m (Ellsworth *et al.,* 2018; Clemente-Moreno *et al.,* 2019; Carriquí *et al.,* 2020; Roig-Oliver *et al.,* 2020). This likely occurs due to the complex covalent and non-covalent interactions between cell wall components changing cell wall porosity, the capacity for molecular movement through the cell wall, and therefore altering the ability of CO_2 to diffuse through the cell wall to the chloroplast (Evans *et al.,* 2009; Terashima *et al.,* 2011)., The importance of cell wall porosity in determining g_m is evident through modeling studies, in which g_m predicted from leaf anatomical traits only measuring the distance of CO_2 diffusion often differ from the actual measured g_m from the gas exchange method (Tosens and Laanisto, 2018). As cell wall compositions differ among plant taxa, cell types, and developmental stages (Popper *et al.,* 2011; Voiniciuc *et al.,* 2018), an interesting future avenue for research could be to analyze how specific chemical and structural changes to cell walls impact 3D leaf architecture and g_m. EM quantification of cell wall thickness could be coupled to biochemical imaging of cell wall composition to get a more complete picture of how cell wall dynamics influence g_m (see next section for advancement in cell wall biochemical imaging).

Leaf internal light environment: The amount of photosynthetically active radiation -PAR, 400–750 nm - absorbed (McCree, 1971; Zhen and Bugbee, 2020), reflected, scattered, or transmitted by leaf depends on leaf architecture and chemical properties. Similar to CO_2 diffusion, the path that light takes from the epidermis to a chloroplast is influenced by leaf thickness; position and abundance of chloroplasts; shape and distribution of IAS; and organization of non-photosynthetic cells such as epidermis, hypodermis, and bundle sheath extension, that altogether contribute to the optical properties of the leaf (Allen *et al.,* 1970; McClendon, 1984; Karabourniotis *et al.,* 2000; Earles *et al.,* 2017; Ustin and Jacquemoud, 2020). Individual chloroplasts experience different light angles or intensities depending on their position in the cell and the depth of the cells in the leaf tissue (Vogelmann and Evans, 2002; Evans and Vogelmann, 2006; Borsuk and Brodersen, 2019) and in response to the intensity and the angle of light change their position inside the cell (Kasahara *et al.,* 2002; Wada *et al.,* 2003; Suetsugu and Wada, 2005; Li *et al.,* 2009; Yamada *et al.,* 2009; Maai *et al.,* 2011; Casal, 2013; Kirchhoff, 2019). Chloroplast arrangement and pigment content also influence the behavior and quality of light penetrating to the deeper layers of photosynthetic cells by shading the lower chloroplast or absorbing the red and blue light, leaving the abaxial chloroplasts mostly with the green light (Terashima and Inoue, 1984, 1985; Terashima *et al.,* 2009).

The bulk of our knowledge on the spatial distribution of photosynthetic pigments inside cell layers has been derived from chlorophyll fluorescence in leaf cross-sections (Vogelmann and Evans, 2002; Brodersen and Vogelmann, 2010; Slattery *et al.,* 2016; Borsuk and Brodersen, 2019). Ideally, *in vivo* experiments reflect the dynamics of chloroplast interaction with light and its influence on the quality and intensity of light being transferred to the abaxial leaf side. Light-sheet fluorescent microscopes are a powerful tool for live imaging (Table 1). But the perpendicular arrangement of illumination and detection objectives provides a diagonal plane of focus not fully adaptable to the requirements of experiments designed to profile the light penetration gradient from adaxial to abaxial leaf face. As well, samples such as broadleaves hardly fit into the small sample chamber. This, in addition to tissue preparation requirements (Ovecka *et al.,* 2015), leaves researchers to perform

light-sheet microscopy on a cross-section with the leaf illuminated from the adaxial and or adaxial side and the fluorescence detected by an object perpendicular to the cross-section (Slattery *et al.,* 2016; Lichtenberg *et al.,* 2017). Light-sheet derivative innovations such as single-objective methods could be considered as a solution (Strack, 2021).

To detect chloroplast movement in *vivo*, Ryu *et al.* (2014) imaged leaves from the C_4 species maize and sorghum to a depth of 100 µm and confirmed the dynamic movement of mesophyll chloroplasts and static behavior of bundle sheath chloroplasts in response to the transition from dark to blue light using two-photon microscopy. However, the same approach may pose more challenges when a C_3 broadleaf such as tobacco or sunflower is examined. C_3 leaves are usually thicker, contain more mesophyll cells with a higher number of chloroplasts per cell (Edwards and Voznesenskaya, 2011; Stata *et al.,* 2014) that could increase the optical density of the leaves greater than the leaves of thin C_4 grasses such as sorghum. Methods to overcome this challenge are still expected to be developed.

Non-destructive technologies to measure the chemical composition and concentration of cells are required to predict light behavior in green leaves. Formed by leaf age and environmental conditions, the leaf chemical composition determines leaf optical properties. The leaf chemical composition includes leaf water content, the concentration of secondary metabolites; and the deposition of cutin, wax, and secondary cell wall components such as crystalline cellulose, suberin, lignin, and other phenolics (Talamond *et al.,* 2015; Donaldson, 2020; Ustin and Jacquemoud, 2020 and references within). Since extraction of cellular compounds such as cellulose modifies the 3D structures of the molecules and removes them from their position, *in vivo* assessment of molecules inside the leaf tissue would provide a direct assessment of the spatial distribution and structure of chemicals (Ustin and Jacquemoud, 2020). Such assessments are becoming more possible for non-fluorescing chemicals by the development of advanced techniques in chemical imaging such as vibrational micro-spectroscopy (see the following section).

4- Beyond the structure: Where are the molecules located?

The daily activities of a leaf cell include the fast turnover and movement of metabolites, as well as biosynthesis, localization, and degradation of proteins and enzymes. Spatially resolving the dynamics of these proteins and metabolites is essential to understanding the efficiency of photosynthesis, particularly when plant breeding research targets the enhancement, reduction, or re-localization of protein and metabolite synthesis or trafficking in the leaf. Examples include introducing carbon concentration mechanisms into C_3 crops, introducing photosynthesis to non-plant organisms, engineering photorespiratory bypass pathways, and optimizing photosynthetic responses to environmental conditions (Schuler *et al.,* 2016; Orr *et al.,* 2017; Batista-Silva *et al.,* 2020). Currently, available methods for spatial assessment of cellular proteins and metabolites (addressed in the following section) range from immunohistochemistry and *in vivo* monitoring of fluorescent reporters to chemical characterization of cell components by mass spectrometry imaging (MSI), X-ray spectroscopy imaging, and vibrational micro-spectroscopy.

Protein localization

The development of poly- and monoclonal antibodies and immunohistochemistry have enabled spatially tracing proteins and biomolecules in photosynthetic research as a discovery or phenotyping tool. Limited examples include localization of photosystems (PSI and PSII) and light-harvesting complexes and identification of cell and organelle-specific distribution of photosynthetic and photorespiratory enzymes (Vallon *et al.,* 1987; Vaughn, 1987; Ueno, 1998; Edwards *et al.,* 2001; Khoshravesh *et al.,* 2016, 2020; Kramer *et al.,* 2021). Immunolabeling detects proteins and biomolecules with a high resolution; co-labeling of multiple proteins and biomolecules is feasible by using multiple-sized gold-conjugated secondary antibodies when immunolabeling is performed on

ultrathin sections and observed by TEM (Foissner and Hoeftberger, 2019), or primary or secondary antibodies conjugated to fluorophores with non-overlapping emission wavelength; and is compatible with TOC for volume visualization (Palmer *et al.,* 2015). Applying the PEA-CLARITY TOC method, Danila *et al.* (2016, 2018) analyzed the plasmodesmata distribution between mesophyll and bundle sheath cells in a variety of grass species by immunolabeling of β-1,3-glucan (callose) in a 3D view of 350 μm^2 area X 100 µm leaf thickness, which represents the cellular plasmodesmatal connection more accurately than 50-70 nm EM sections. But antibodies poorly diffuse into the whole mount tissue potentially due to the cuticle and cell wall acting as a barrier. While enhancing tissue permeabilization with partial cell wall digestion may facilitate antibody infiltration into the macerated cells or the tissue, immunolabeling still requires a very high concentration of antibodies, long incubations, or vacuum infiltration (Chuong *et al.,* 2006; Danila *et al.,* 2016) which could cause non-specific binding and make immunolabeling of leaf tissue a difficult daily task. As well, immunolabeling works with aldehyde-fixed tissue making *in vivo* immunolabeling impossible.

Engineering fluorescent proteins has improved the limitations of poor antibody performance and restrictions of immunolabeling in live imaging (Hanson and Kohler, 2001). Fluorescent tagging allows visualization of endogenous or engineered proteins inside the whole plant body, estimates subcellular target protein localization with over 80% accuracy, and signals the dynamic nature of subcellular interactions between multiple protein tags (Ckurshumova *et al.,* 2011; Tanz *et al.,* 2013; Delfosse *et al.,* 2016). However, both immunolabeling and fluorescent proteins restrict the experiments to a few fluorophores that do not interfere with the red emission of chlorophylls; to the proteins and biomolecules that an antibody has been developed for, *i.e*. has a characterized specificity for a given epitope; or few model plants with established transformation protocols, thus eliminating non-model organisms that are hard to genetically engineer (Ziemienowicz, 2014; Chen *et al.,* 2020).

Mass spectrometry imaging (MSI)

MSI is an emerging technique to spatially detect proteins, lipids, and metabolites (Caldwell and Caprioli, 2005; Miura *et al.,* 2012; Bartels and Svatoš, 2015; Boughton *et al.,* 2016). Mass spectrometry inherently applies multiple levels of destruction - freezing, grinding, digestion, extraction, and metabolite or protein profiling methods such as ionization and UV laser disruption, which remove biomolecules from their natural position (Freund and Hegeman, 2017; Alseekh *et al.,* 2018). MSI overcomes these limits by corresponding the identified molecules to an image pixel by pixel. Sample preparation for MSI could be as minimal as embedding the tissue in a media, cross-sectioning -usually cryo-sectioning- and subjecting the section to the ion source and mass analyzer. When the ion source, the mass analyzer, and the detector are placed in a microprobe, the sampling probe moves across an XY direction and profiles the mass spectra corresponding to the XY on the cross-section (Boughton *et al.,* 2016; Dong *et al.,* 2016). Using serial sections of four germinating stages of maize seeds from B73 and Mo17 inbreds and application of MSI, Feenstra *et al*. (2017) classified differences between the abundance and distribution pattern of molecular groups such as phospholipids, respiratory metabolites, organic and amino acids in 3D. 3D MSI is also possible by adjusting the height of the probe and moving it repeatedly across the surface of thick tissue, removing successive layers until the desired depth/volume has been analyzed (Buchberger *et al.,* 2018). MSI is also label-free as well as compatible with stable isotope labeling that enables *in situ* kinetic analysis (Louie *et al.,* 2013). But, when applying MSI methods, the tissue must be subjected to ionization and mass analyzer instruments (Dong *et al.,* 2016); processes that take apart the tissue molecule by molecule. Thus, MSI may have already reached its full capability in the detection of spatial metabolite dynamics *in vivo*.

Micro-spectroscopy

Currently, the most successful non-destructive approaches in molecular imaging are based on micro-spectroscopy. Spectroscopy is described as the assessment of the intensity and pattern of electromagnetic waves absorbed or emitted in interaction with matter. This fundamental molecular characteristic has led to the development of multiple spectroscopy techniques with a long history of implementation in physics, chemistry, astronomy, and more recently in biology (Ball and Engineers., 2006). Spectroscopy imaging by microscopes (micro-spectroscopy) collects spectra of an object in point, line, or XY dimensions and enables (bio)chemical analysis of the object by spectral characterization, localization, and classification without chemical extraction. Ideally, to map cell (bio)chemistry *in vivo*, impose the least interruption to the cell metabolism, and capture the cell dynamics over time, a micro-spectroscopy technique should be label-free and use a source of relatively low energy radiation that inflicts the least destruction to the cellular metabolism. As well, the technique must be capable of 1) imaging molecules in a cellular aqueous environment, 2) covering a large sample size with high lateral and depth resolution, 3) identifying structural and functional molecules - ideally at the individual molecules sensitivity, and 4) imaging time series at a speed competing with the speed of metabolite movement and turnover. Some techniques that meet more than one of these criteria and have been implemented in leaf molecular imaging are X-ray spectroscopy imaging (Donner *et al.,* 2012; Vijayan *et al.,* 2015; Kopittke *et al.,* 2018) and vibrational spectroscopy including Fourier Transform Infrared (FT-IR) and Raman micro-spectroscopy (Salzer and Siesler, 2014).

X-ray spectroscopy imaging

X-ray spectroscopy (XRS) imaging relies on the X-ray absorption or fluorescence emission of the elements (Box 2). X-ray fluorescence microscopy (SR-XFM) was first applied in plant chemical analysis during 1990s (Kopittke *et al.,* 2018) to map and quantify the spatial concentration of metals for toxicity, hyperaccumulation, and elemental composition analysis (Berglund *et al.,* 1999;

Fukumoto *et al.,* 1999; Pickering *et al.,* 2000; Sarret *et al.,* 2003). The advancements in the speed of fluorescence detectors, the power of X-ray penetration in the whole tissue, and the capability of XFM in detecting a very low concentration of the target element has made SR-XFM a powerful *in vivo* tool in ionomics – mineral nutrient and trace elemental composition of a living organism in response to environmental conditions, developmental stage, and genetic background (Salt *et al.,* 2008; Punshon *et al.,* 2013). As well, XFM plays a substantial phenotyping role in analyzing trace metal metabolism and understanding the function of the genes regulating elemental homeostasis by *in vivo* elemental imaging with the resolutions less than one micrometer and time resolution as short as milliseconds (Donner *et al.,* 2012; Kopittke *et al.,* 2018).

Trace elements are indispensable for photosynthesis and respiration, during the catalytic cycle, and developmental processes. For example, the whole length of the electron transport chain from PSII to cytochrome b, PSI complexes, and ferredoxin depend on different forms of Fe complexes; Cu exists in plastocyanin; and Fe, Mn, Cu, or Zn play a role in water splitting reaction in PS II of the oxygen-evolving photosynthetic organisms (Raven *et al.,* 1999 and references within). Trace elements such as Mn, Fe, Ca, and Zn are also involved in chloroplast development, chlorophyll biosynthesis, cuticular wax deposition, and signaling (Alejandro *et al.,* 2020 and references within; Raven *et al.,* 1999 and references within; Tripathy and Pattanayak, 2012). While essential for the proper functioning of photosynthesis, non-optimal exposure to trace elements could cause toxicity or deficiency (Palit *et al.,* 1994; Kopittke *et al.,* 2014; Andresen *et al.,* 2018; Blamey *et al.,* 2018; Paunov *et al.,* 2018). Parallel to the development of modern approaches such as nano-fertilizers or crops bred for optimal trace metal metabolism to address global micronutrients (*e.g.* Zn) deficiency and soil heavy metal contamination, XRS imaging is a promising phenotyping approach to detect whether the crop species uptake, relocate, metabolize, and store micronutrients efficiently for improved photosynthetic function or human consumption (Donner *et al.,* 2012; Kopittke *et al.,* 2018; Raliya *et al.,* 2018).

XRS imaging is fast and accurate and is sensitive to the oxidative state of the elements. The element-specificity of XRS allows visualizing small quantities of the target elements in a matrix of macromolecules such as within a photosynthetic cell. XFM combined with micro-CT also allows collecting the distribution of the elements in leaf 3D structure (Donner *et al.,* 2012). However, repeated exposure to the high-energy X-ray could increase ionization level and pose damage to the metabolism, increase intracellular ROS level, change the elemental oxidation status, and modify elemental transport and trafficking and consequently interfere with the *in vivo* experiments (Dixit and Cyr, 2003; Vijayan *et al.,* 2015). XRS imaging also faces limitations in the identification of elements with atomic numbers less than 11 -which includes the main building blocks of biological material: carbon, nitrogen, and oxygen (Pushie *et al.,* 2014). And finally, XRS is useful for localization and quantification of elements within plant cells not for detecting larger macromolecules and metabolites which limits its scope in detecting photosynthetic traits in 3D leaf tissues.

Vibrational micro-spectroscopy

Vibrational micro-spectroscopy – Infrared (IR) absorption and Raman scattering - are two widely implemented non-destructive and label-free chemical analysis techniques that rely on the interaction between light and the vibrational energy of molecular bonds (Lasch and Kneipp, 2008). Each molecule has a unique atomic composition and the classes of biomolecules (*e.g.* proteins) contain functional groups (*e. g.* amine and carboxylic groups). Both IR and Raman micro-spectroscopy detect functional groups and molecular fingerprints unique to the (macro/bio) molecule of interest (Gierlinger and Schwanninger, 2007; Türker-Kaya and Huck, 2017; Zhao *et al.,* 2019). Different in principle (Box 3), IR and Raman micro-spectroscopy allow spatial characterization and classification of biomolecules in a targeted and untargeted approach, simultaneously detect a wide range of macromolecules in a biochemically complex biological system (Figure 4), and require minimal sample preparation (Salzer and Siesler, 2014; Beć *et al.,* 2020).

A great advantage of vibrational spectroscopy is that all biochemical information of the cells is collected with one imaging attempt. As a result, each hyperspectral image contains a pool of unidentified spectra (Figure 4); when 3D imaging, this pool is amplified by the magnitude of the z-dimension. Consequently, the identification and classification of biomolecules heavily rely on 1) the previously created spectral reference libraries of individual purified molecules, and 2) the development of algorithms for classification or isolation of spectra corresponding to a single or a group of biomolecules. While the spectral libraries of inorganic chemicals are maturing and becoming publicly available in the form of interactive spectra as by Infrared and Raman Using Group (http://www.irug.org), the spectral libraries for the single and groups of biomolecules are finding their way into publications (Socrates and Socrates, 2000; De Gelder *et al.,* 2007; Zhu *et al.,* 2011; Wiercigroch *et al.,* 2017). Concurrently, algorithms for spectral smoothing and background correction, as well as statistical models for multivariate analysis of hyperspectral images, such as principal component analysis (PCA) and multivariate curve resolution–alternating least squares (MCR-ALS, Figure 4), have been adopted to evaluate and interpret complex hyperspectral data (Gautam *et al.,* 2015; Felten *et al.,* 2015; Olmos *et al.,* 2017; Smith *et al.,* 2019). However, this dependence of data analysis on advanced statistical models and computational power creates a demand for better computational skills and greater storage and analysis space. To further advance this method of imaging, the development of scripts and quantification pipelines in open-source software such as Python and R, as well as user-friendly applications with graphical user interface (GUI) will be needed.

Integration of vibrational micro-spectroscopy into plant cell biology is still in its infancy. High-resolution IR spectroscopy - up to 4 cm^{-1} spectral and 1.56 µm lateral resolution and 1 cm sec^{-1} scanning speed- has been applied to classify subcellular components such as starch grains, protein bodies, and chloroplasts; to differentiate between α-helix and β-sheet of proteins and between structural and non-structural carbohydrates; to determine the biochemical states of macromolecules (*e.g.* methylation levels of pectin); and to identify the secondary structure of proteins, lipids and lipid

droplets, and secondary metabolites (*e.g.* flavonoids, terpenoids, and alkaloids) based on their characteristic IR bands (Wetzel *et al.,* 2003; Jamme *et al.,* 2013; Krähmer *et al.,* 2013; Mazurek *et al.,* 2013; Tanino *et al.,* 2013; Xin *et al.,* 2013; Warren *et al.,* 2015). Raman micro-spectroscopy has been used successfully to spatially identify - up to 1 cm^{-1} spectral, and 0.47 µm lateral resolution, quantify plant pigments -*e.g.* chlorophylls and carotenoids (Collins *et al.,* 2011; Moudříková *et al.,* 2016; Meeßen *et al.,* 2017; Koch *et al.,* 2017; Yang *et al.,* 2017; Vítek *et al.,* 2020), and localize and quantify subcellular levels of polyphosphates (Moudříková *et al.,* 2017), cyanogenic glycosides (Krafft *et al.,* 2012; Heraud *et al.,* 2018), and plant secondary metabolites such as alkaloids, cannabinoids, terpenes and phenolic compounds (Vaverkova *et al.,* 2014; Belt *et al.,* 2017; Ebersbach *et al.,* 2018; Midorikawa *et al.,* 2020). Due to the ability of vibrational micro-spectroscopy to characterize the molecular structure of biopolymers in primary and secondary cell walls non-destructively, these techniques have revolutionized the study of the chemical composition in the plant cell wall and cuticle (Dokken *et al.,* 2005; Gierlinger *et al.,* 2013; Gierlinger, 2018; Zhao *et al.,* 2019). Considering the significance of cell wall biochemical composition in mesophyll geometry and CO_2 diffusivity (See section 3), vibrational spectroscopy and its potentials for discovery could lead the way for another revolution in photosynthesis research. The example Raman hyperspectral microscopy in Figure 4 indicates the presence of lignin-like phenolic polymers in *Sphagnum* leaf cell walls. Although immunohistochemistry (Ligrone *et al.,* 2008), IR spectroscopy (Farmer and Morrison, 1964), acid hydrolysis-resistant (Graham *et al.,* 2004) and bioinformatics (Weng and Chapple, 2010) have previously provided direct and indirect evidence that lignin-like phenolic compounds exist in bryophytes, histological staining such as Phloroglucinol-HCl has shown negative results for lignin (Kremer *et al.,* 2004). To understand the composition of the cell wall in *Sphagnum*, its effect on retaining water during the early establishment of the land plants, and its influence on the global carbon cycle in moss peatland reservoirs, modern and high-resolution vibrational micro-spectroscopy methods are promising tools.

Compared to the weak and rare Raman effect, IR signals are stronger. When IR is supplied by a synchrotron, the brightness of the radiation improves the signal to noise and the resolution (Wetzel *et al.,* 1998; Vijayan *et al.,* 2015), and the use of synchrotron-based IR has been proved non-toxic to the cellular metabolism in *Chlamydomonas* and human T-cells when time series are obtained (Holman *et al.,* 2002; Goff *et al.,* 2009). But Raman micro-spectroscopy is more optimal for imaging a cellular aqueous environment, as water appears as a strong absorption band in IR spectra and overlaps with some functional groups (Beć *et al.,* 2020). Depth is also less achievable by IR spectroscopy. IR absorption spectroscopy requires very thin (<50 µm) and transparent samples and utilizing external reflection or attenuated total reflectance mode only helps to penetrate the tissue by a few more microns (Beć *et al.,* 2020). Consequently, non-destructive chemical mapping has been implemented on the thin sections of plant organs such as wheat or *Arabidopsis* leaves (Xin *et al.,* 2013; Warren *et al.,* 2015), single living organisms such as *Chlamydomonas reinhardtii* (Goff *et al.,* 2009), or very thin or transmitting organs such as Arabidopsis petals and single epidermis layers of *Allium* (Mazurek *et al.,* 2013; Tanino *et al.,* 2013). On the contrary, Raman micro-spectroscopy could be coupled with confocal setups to add depth to the imaging (Gomes da Costa *et al.,* 2019). However, the Raman effect is weak and requires longer acquisition times or higher laser intensities. Point and line scanning by confocal Raman micro-spectroscopes may take hours to scan the depth of tissue and the higher energy lasers (UV and 532 nm) or longer acquisition times could burn the tissue due to excessive local temperature rise (Butler *et al.,* 2016). Recently, applying light-sheet illumination has increased the speed of imaging 213 times by reducing the time required to collect 4 million Raman spectra from 51 h (when scanned by confocal Raman microscope) to only 14 minutes. This higher speed eliminated the local heating effect of longer excitation periods (Müller *et al.,* 2016). Another problem with UV and 532 nm lasers is that the Raman signal could be masked by fluorescent from the materials (Wei *et al.,* 2015), causing serious problems for imaging fluorescing tissues such as leaves. Using near-infrared wavelength lasers (785 and 1064 nm) has improved the Raman signal by eliminating fluorescence and reducing the local thermal heating of the tissue thus

making Raman more optimized for imaging leaves (Gierlinger and Schwanninger, 2007; Yang *et al.,* 2013; Heraud *et al.,* 2018).

In plant cells, large vacuoles restrict most of the cellular metabolism to the very narrow area of the cytoplasm sandwiched between the cell membrane and tonoplast, thus a greater spatial resolution is required for imaging. Recently, high-resolution (0.5 µm spatial resolution) Raman hyperspectral imaging has enabled localization of cyanogenic glucosides in the cytoplasm of sorghum coleoptile cells (Heraud *et al.,* 2018). The high resolution and specificity in molecular identification, the capacity to identify both structural and functional molecules, the current technological advancement in Raman micro-spectroscopy such as the development of near-IR lasers, Raman confocal and light-sheet, and the capability of Raman micro-spectroscopy in recognizing metabolites with stable isotope labeling (Li *et al.,* 2013), lists Raman spectroscopy as a future candidate for the development of methods to reconstruct the leaf 3D structure and simultaneously trace metabolic pathways *in vivo*. Such methods will be directly applicable in research that questions metabolite transfer and the speed and dynamics of pathways spatially, for instance, the spatially and temporally resolved $^{13}CO_2$ integration into the C_4 photosynthesis metabolism (Arrivault *et al.,* 2017).

Conclusion

The ability of the photosynthetic organs to capture and convert solar energy to carbohydrates while efficiently managing their access to CO_2, water, and minerals relies on the cellular and subcellular organization of photosynthetic machinery inside the photosynthetic organs - usually a leaf. The accurate estimation of the leaf structure and function can inform a wide range of plant physiology interests from leaf models that promise more efficient photosynthesis (Covshoff and Hibberd, 2012; Tholen *et al.,* 2012; Leegood, 2013; Ren *et al.,* 2019; Lundgren and Fleming, 2020) to the urban solar cells that simulate leaf structure for more efficient energy trapping (Yun *et al.,* 2019). Here, we reviewed some common approaches in outlining leaf structure and biochemical composition and the optical and structural complexity of the green leaves. While there is not yet a

single best solution that could be performed to accurately estimate leaf structure in large and small scales and evaluate the leaf dynamic structural and biochemical response to the environmental fluctuation, there are multiple complementary techniques available depending on the research hypothesis, the expected details and accuracy, budget, and accessible resources. Over the past two decades, the ever-growing interest in imaging 3D cells and tracking *in vivo* cell dynamics have led to the blooming of innovations that integrate the modern concepts of optical and quantum physics, biochemistry, mathematics, statistics, and machine learning to shed more light on the unknown facts inside the leaf. With all these innovations, we have never been as powerful and as close to understanding the mechanisms of what Grew (1682)called *"the methods which nature takes to preserve them [leaves] from the injuries both of the ground and of the weather*".

Acknowledgments

This review was supported by funding from DOE BER grant number DE-SC0019267 and NSF grant number DEB 1737899.

Author Contribution

All authors contributed to conceptualization, writing, reviewing, and editing. RK drafted the manuscript and prepared the figures and graphs.

References

Aalto T, Juurola E. 2002. A three-dimensional model of CO_2 transport in airspaces and mesophyll cells of a silver birch leaf. Plant, Cell and Environment **25**, 1399–1409.

Adão T, Hruška J, Pádua L, Bessa J, Peres E, Morais R, Sousa JJ. 2017. Hyperspectral imaging: A review on UAV-based sensors, data processing and applications for agriculture and forestry. Remote Sensing **9**, doi:10.3390/rs9111110.

Adur J, Carvalho HF, Cesar CL, Casco VH. 2016. Nonlinear Microscopy Techniques: Principles and Biomedical Applications. In: Stanciu SG, ed. Microscopy and Analysis. IntechOpen, 121–124.

Alejandro S, Höller S, Meier B, Peiter E. 2020. Manganese in Plants: From Acquisition to Subcellular Allocation. Frontiers in Plant Science **11**, 1–23.

Allard G, Nelson CJ, Pallardy SG. 1991. Shade Effects on Growth of Tall Fescue: I. Leaf Anatomy and Dry Matter Partitioning. Crop Science **31**, 163–167.

Allen WA, Gausman HW, Richardson AJ. 1970. Mean Effective Optical Constants of Cotton Leaves. Journal of the Optical Society of America **60**, 542.

Alseekh S, Bermudez L, de Haro LA, Fernie AR, Carrari F. 2018. Crop metabolomics: from diagnostics to assisted breeding. Metabolomics **14**, 1–13.

Ambrose C, DeBono A, Wasteneys G. 2013. Cell geometry guides the dynamic targeting of apoplastic GPI-linked lipid transfer protein to cell wall elements and cell borders in Arabidopsis thaliana. PLoS ONE **8**, 1–13.

Amigo JM, Babamoradi H, Elcoroaristizabal S. 2015. Hyperspectral image analysis. A tutorial. Analytica Chimica Acta **896**, 34–51.

Andresen E, Peiter E, Küpper H. 2018. Trace metal metabolism in plants. Journal of Experimental Botany **69**, 909–954.

Arrivault S, Obata T, Szecówka M, Mengin V, Guenther M, Hoehne M, Fernie AR, Stitt M. 2017. Metabolite pools and carbon flow during C_4 photosynthesis in maize: $^{13}CO_2$ labeling kinetics and cell type fractionation. Journal of Experimental Botany **68**, 283–298.

Austin JR, Staehelin AL. 2011. Three-dimensional architecture of grana and stroma thylakoids of higher plants as determined by electron tomography. Plant Physiology **155**, 1601–1611.

Ayache J, Beaunier L, Boumendil J, Ehret G, Laub D. 2012. *Sample Preparation Techniques for Transmission Electron Microscopy* (J Ayache, Ed.). Springer New York.

Baillie AL, Baillie AL, Fleming AJ. 2019. The developmental relationship between stomata and mesophyll airspace. New Phytologist **225**, 1120–1126.

Baillon H. 1882. *Anatomie et physiologie végétales*. Paris: Hachette.

Baker A, Sparkes IAA, Brown L-AA, O'Leary-Steele C, Warriner SLL. 2010. Peroxisome biogenesis and positioning. Biochemical Society Transactions **38**, 807–816.

Ball DW, Engineers. S of PI. 2006. *Field guide to spectroscopy*. Bellingham, Wash: SPIE.

Bartels B, Svatoš A. 2015. Spatially resolved in vivo plant metabolomics by laser ablation-based mass spectrometry imaging (MSI) techniques: LDI-MSI and LAESI. Frontiers in Plant Science **6**, 1–7.

Batista-Silva W, da Fonseca-Pereira P, Martins AO, Zsögön A, Nunes-Nesi A, Araújo WL. 2020. Engineering Improved Photosynthesis in the Era of Synthetic Biology. Plant Communications **1**, 1–17.

Beć KB, Grabska J, Bonn GK, Popp M, Huck CW. 2020. Principles and Applications of Vibrational Spectroscopic Imaging in Plant Science: A Review. Frontiers in Plant Science **11**, 1–27.

Bell K, Oparka K. 2011. Imaging plasmodesmata. Protoplasma **248**, 9–25.

Belt T, Keplinger T, Hänninen T, Rautkari L. 2017. Cellular level distributions of Scots pine heartwood and knot heartwood extractives revealed by Raman spectroscopy imaging. Industrial

Crops and Products **108**, 327–335.

Berglund A, Brelid H, Rindby A, Engström P. 1999. Spatial Distribution of Metal Ions in Spruce Wood by Synchrotron Radiation Microbeam X-Ray Fluorescence Analysis. Holzforschung Wood Research and Technology **53**, 474-480.

Blackman FF, Darwin F. 1895. XI. Experimental researches on vegetable assimilation and respiration.—No. II. On the paths of gaseous exchange between aerial leaves and the atmosphere. Philosophical Transactions of the Royal Society of London. (B.) **186**, 503–562.

Blamey FPC, McKenna BA, Li C, *et al.* 2018. Manganese distribution and speciation help to explain the effects of silicate and phosphate on manganese toxicity in four crop species. New Phytologist **217**, 1146–1160.

Bolhàr-Nordenkampf HR, Draxler G. 1993. Functional leaf anatomy. In: Hall D, Scurlock J, Bolhàr-Nordenkampf H, Leegood R, Long S, eds. Photosynthesis and Production in a Changing Environment: A field and laboratory manual. Dordrecht: Springer Netherlands, 91–112.

Borsuk AM, Brodersen CR. 2019. The spatial distribution of chlorophyll in leaves. Plant Physiology **180**, 1406–1417.

Boughton BA, Thinagaran D, Sarabia D, Bacic A, Roessner U. 2016. Mass spectrometry imaging for plant biology: a review. Phytochemistry Reviews **15**, 445–488.

Brodersen CR, Vogelmann TC. 2010. Do changes in light direction affect absorption profiles in leaves? Functional Plant Biology **37**, 403–412.

Broess K, Borst JW, Van Amerongen H. 2009. Applying two-photon excitation fluorescence lifetime imaging microscopy to study photosynthesis in plant leaves. Photosynthesis Research **100**, 89–96.

Buchberger AR, DeLaney K, Johnson J, Li L. 2018. Mass Spectrometry Imaging: A Review of Emerging Advancements and Future Insights. Analytical Chemistry **90**, 240–265.

Busch FA, Sage TL, Cousins AB, Sage RF. 2013. C_3 plants enhance rates of photosynthesis by reassimilating photorespired and respired CO_2. Plant Cell and Environment **36**, 200–212.

Bussi Y, Shimoni E, Weiner A, Kapon R, Charuvi D, Nevo R, Efrati E, Reich Z. 2019. Fundamental helical geometry consolidates the plant photosynthetic membrane. Proceedings of the National Academy of Sciences of the United States of America **116**, 22366–22375.

Butler HJ, Ashton L, Bird B, *et al.* 2016. Using Raman spectroscopy to characterize biological materials. Nature Protocols **11**, 664–687.

Caldwell RL, Caprioli RM. 2005. Tissue profiling by mass spectrometry: A review of methodology and applications. Molecular and Cellular Proteomics **4**, 394–401.

Capua Y, Eshed Y. 2017. Coordination of auxin-triggered leaf initiation by tomato LEAFLESS. Proceedings of the National Academy of Sciences of the United States of America **114**, 3246–3251.

Carriquí M, Nadal M, Clemente-Moreno MJ, Gago J, Miedes E, Flexas J. 2020. Cell wall composition strongly influences mesophyll conductance in gymnosperms. Plant Journal **103**, 1372–1385.

Casal JJ. 2013. Photoreceptor signaling networks in plant responses to shade. Annual Review of Plant Biology **64**, 403–427.

Chater CCC, Caine RS, Fleming AJ, Gray JE. 2017. Origins and Evolution of Stomatal Development. Plant Physiolgy **174**, 624–638.

Chen Y, Mao W, Liu T, Feng Q, Li L, Li B. 2020. Genome Editing as A Versatile Tool to Improve Horticultural Crop Qualities. Horticultural Plant Journal **6**, 372–384.

Chen X, Wen J. 2012. In situ wet-cell TEM observation of gold nanoparticle motion in an aqueous solution. Nanoscale Research Letters **7**, 1–6.

Chuong SDX, Franceschi VR, Edwards GE. 2006. The cytoskeleton maintains organelle partitioning

required for single-cell C_4 photosynthesis in Chenopodiaceae species. Plant Cell **18**, 2207–2223.

Cisek R, Spencer L, Prent N, Zigmantas D, Espie GS, Barzda V. 2009. Optical microscopy in photosynthesis. Photosynthesis Rsearch **102**, 111–141.

Ckurshumova W, Caragea AE, Goldstein RS, Berleth T. 2011. Glow in the dark: Fluorescent proteins as cell and tissue-specific markers in plants. Molecular Plant **4**, 794–804.

Clarke VC, Danila FR, Von Caemmerer S. 2021. CO2 diffusion in tobacco: A link between mesophyll conductance and leaf anatomy. Interface Focus **11**, 20200040. doi:10.1098/rsfs.2020.0040.

Clemente-Moreno MJ, Gago J, Díaz-Vivancos P, Bernal A, Miedes E, Bresta P, Liakopoulos G, Fernie AR, Hernández JA, Flexas J. 2019. The apoplastic antioxidant system and altered cell wall dynamics influence mesophyll conductance and the rate of photosynthesis. Plant Journal **99**, 1031–1046.

Collins AM, Jones HDT, Han D, Hu Q, Beechem TE, Timlin JA. 2011. Carotenoid distribution in living cells of haematococcus pluvialis (Chlorophyceae). PLoS ONE **6**, 1–7.

Collins AM, Liberton M, Jones HDT, Garcia OF, Pakrasi HB, Timlin JA. 2012. Photosynthetic pigment localization and thylakoid membrane morphology are altered in Synechocystis 6803 phycobilisome mutants. Plant Physiology **158**, 1600–1609.

Coulter JM, Barnes CR, Cowles HC. 1910. *A textbook of botany for colleges and universities*. New York: American book company.

Covshoff S, Hibberd JM. 2012. Integrating C_4 photosynthesis into C_3 crops to increase yield potential. Curr Opin Biotechnol **23**, 209–214.

Crawford AJ, Mclachlan DH, Hetherington AM. 2012. High temperature exposure increases plant cooling capacity. Current Biology **22**, R396–R397.

Crumpton-Taylor M, Grandison S, Png KMY, Bushby AJ, Smith AM. 2012. Control of starch granule

numbers in Arabidopsis chloroplasts. Plant Physiology **158**, 905–916.

Danila FR, Quick WP, White RG, von Caemmerer S, Furbank RT. 2019. Response of plasmodesmata formation in leaves of C_4 grasses to growth irradiance. Plant Cell and Environment **42**, 2482–2494.

Danila FR, Quick WP, White RG, Furbank RT, von Caemmerer S. 2016. The Metabolite Pathway between Bundle Sheath and Mesophyll: Quantification of Plasmodesmata in Leaves of C_3 and C_4 Monocots. The Plant Cell **28**.

Danila FR, Quick WP, White RG, Kelly S, Von Caemmerer S, Furbank RT. 2018. Multiple mechanisms for enhanced plasmodesmata density in disparate subtypes of C_4 grasses. Journal of Experimental Botany **69**, 1135–1145.

Danila FR, Thakur V, Chatterjee J, Bala S, Coe RA, Acebron K, Furbank RT, von Caemmerer S, Quick WP. 2021. Bundle sheath suberisation is required for C_4 photosynthesis in a Setaria viridis mutant. Communications Biology **4**, 1–10.

Datta R, Heaster TM, Sharick JT, Gillette AA, Skala MC. 2020. Fluorescence lifetime imaging microscopy: fundamentals and advances in instrumentation, analysis, and applications. Journal of Biomedical Optics **25**, 071203.

Daum B, Kühlbrandt W. 2011. Electron tomography of plant thylakoid membranes. Journal of Experimental Botany **62**, 2393–2402.

Delfosse K, Wozny MR, Jaipargas EA, Barton KA, Anderson C, Mathur J. 2016. Fluorescent protein aided insights on plastids and their extensions: A critical appraisal. Frontiers in Plant Science **6**, 1–22.

Dixit R, Cyr R. 2003. Cell damage and reactive oxygen species production induced by fluorescence microscopy: Effect on mitosis and guidelines for non-invasive fluorescence microscopy. Plant Journal **36**, 280–290.

Dokken KM, Davis LC, Marinkovic NS. 2005. Use of infrared microspectroscopy in plant growth and

development. Applied Spectroscopy Reviews **40**, 301–326.

Donaldson L. 2020. Autofluorescence in plants. Molecules **25**.

Dong Y, Li B, Malitsky S, Rogachev I, Aharoni A, Kaftan F, Svatoš A, Franceschi P. 2016. Sample preparation for mass spectrometry imaging of plant tissues: A review. Frontiers in Plant Science **7**.

Donner E, Punshon T, Guerinot M Lou, Lombi E. 2012. Functional characterisation of metal(loid) processes in planta through the integration of synchrotron techniques and plant molecular biology. Analytical and bioanalytical chemistry **402**, 3287–3298.

Earles JM, Buckley TN, Brodersen CR, *et al.* 2019. Embracing 3D Complexity in Leaf Carbon–Water Exchange. Trends in Plant Science **24**, 15–24.

Earles JM, Théroux-Rancourt G, Gilbert ME, McElrone AJ, Brodersen CR. 2017. Excess diffuse light absorption in upper mesophyll limits CO_2 drawdown and depresses photosynthesis. Plant Physiology **174**, 1082–1096.

Earles JM, Théroux-Rancourt G, Roddy AB, Gilbert ME, McElrone AJ, Brodersen CR. 2018. Beyond porosity: 3D leaf intercellular airspace traits that impact mesophyll conductance. Plant Physiology **178**, 148–162.

Ebersbach P, Stehle F, Kayser O, Freier E. 2018. Chemical fingerprinting of single glandular trichomes of Cannabis sativa by Coherent anti-Stokes Raman scattering (CARS) microscopy. BMC PLANT BIOLOGY **8**, 1–12.

Edwards GE, Franceschi VR, Ku MS, Voznesenskaya E V, Pyankov VI, Andreo CS. 2001. Compartmentation of photosynthesis in cells and tissues of C_4 plants. J Exp Bot **52**, 577–590.

Edwards GE, Voznesenskaya E V. 2011. C_4 Photosynthesis: Kranz Forms and Single-Cell C_4 in Terrestrial Plants. In: Raghavendra AS, Sage RF, eds. *C_4 photosynthesis and related CO_2 concentrating mechanisms*, Vol. 32. Dordrecht, The Netherlands: Springer Science, 29–61.

Ellsworth P V., Ellsworth PZ, Koteyeva NK, Cousins AB. 2018. Cell wall properties in *Oryza sativa* influence mesophyll CO_2 conductance. New Phytologist **219**, 66–76.

Engel BD, Schaffer M, Cuellar LK, Villa E, Plitzko JM, Baumeister W. 2015. Native architecture of the chlamydomonas chloroplast revealed by in situ cryo-electron tomography. eLife **2015**, 1–29.

Engineer CB, Hashimoto-Sugimoto M, Negi J, Israelsson-Nordström M, Azoulay-Shemer T, Rappel WJ, Iba K, Schroeder JI. 2016. CO_2 Sensing and CO_2 Regulation of Stomatal Conductance: Advances and Open Questions. Trends in Plant Science **21**, 16–30.

Evans JR. 1999. Leaf anatomy enables more equal access to light and CO_2 between chloroplasts. New Phytologist **143**, 93–104.

Evans JR. 2020. Mesophyll conductance: walls, membranes and spatial complexity. New Phytologist.

Evans JR, Von Caemmerer S. 1996. Carbon dioxide diffusion inside leaves. Plant Physiology **110**, 339–346.

Evans JR, von Caemmerer S, Setchell BA, Hudson GS. 1994. The relationship between CO_2 transfer conductance and leaf anatomy in transgenic tobacco with a reduced content of Rubisco. Australian Journal of Plant Physiology **21**, 475–495.

Evans JR, Kaldenhoff R, Genty B, Terashima I. 2009. Resistances along the CO_2 diffusion pathway inside leaves. Journal of Experimental Botany **60**, 2235–2248.

Evans JR, Vogelmann TC. 2006. Photosynthesis within isobilateral Eucalyptus pauciflora leaves. New Phytologist **171**, 771–782.

Farber C, Li J, Hager E, Chemelewski R, Mullet J, Rogachev AY, Kurouski D. 2019. Complementarity of Raman and Infrared Spectroscopy for Structural Characterization of Plant Epicuticular Waxes. ACS OMEGA **4**, 3700–3707.

Farmer VC, Morrison RI. 1964. Lignin in sphagnum and phragmites and in peats derived from these plants. Geochimica et Cosmochimica Acta **28**, 1537–1546.

Feenstra AD, Alexander LE, Song Z, Korte AR, Yandeau-Nelson MD, Nikolau BJ, Lee YJ. 2017. Spatial mapping and profiling of metabolite distributions during germination. Plant Physiology **174**, 2532–2548.

Felten J, Hall H, Jaumot J, Tauler R, de Juan A, Gorzsas A. 2015. Vibrational spectroscopic image analysis of biological material using multivariate curve resolution-alternating least squares (MCR-ALS). NATURE PROTOCOLS **10**, 217–240.

Fisher DG, Ray FE. 1982. Studies on the Leaf of Amaranthus retroflexus (Amaranthaceae): Chloroplast Polymorphism. Botanical Gazette **69**, 1133–1147.

Fitzgibbon J, Bell K, King E, Oparka K. 2010. Super-resolution imaging of plasmodesmata using three-dimensional structured illumination microscopy. Plant Physiology **153**, 1453–1463.

Foissner I, Hoeftberger M. 2019. Chemical Fixation, Immunofluorescence, and Immunogold Labeling of Electron Microscopical Sections BT - Plant Cell Morphogenesis: Methods and Protocols. In: Cvrčková F, Žárský V, eds. New York, NY: Springer New York, 43–62.

Freund DM, Hegeman AD. 2017. Recent advances in stable isotope-enabled mass spectrometry-based plant metabolomics. Current Opinion in Biotechnology **43**, 41–48.

Fujii Y, Ogasawara Y, Takahashi Y, Sakata M, Noguchi M, Tamura S, Kodama Y. 2020. The cold-induced switch in direction of chloroplast relocation occurs independently of changes in endogenous phototropin levels. PLoS ONE **15**, 1–15.

Fukumoto N, Kobayashi Y, Kurahashi M, Kojima I. 1999. X-ray fluorescent spectroscopy with a focused X-ray beam collimated by a glass capillary guide tube and element mapping of biological samples. Spectrochimica acta, Part B: Atomic spectroscopy **54**, 91–98.

Gao L, Smith RT. 2015. Optical hyperspectral imaging in microscopy and spectroscopy – a review of data acquisition. Journal of Biophotonics **8**, 441–456.

Garab G, Faludi-Daniel A, Sutherland JC, Hind G. 1988. Macroorganization of chlorophyll a/b light-harvesting complex in thylakoids and aggregates: information from circular differential scattering. Biochemistry **27**, 2425–2430.

Van Gardingen PR, Jeffree CE, Grace J. 1989. Variation in stomatal aperture in leaves of Avena fatua L. observed by low-temperature scanning electron microscopy. Plant, Cell & Environment **12**, 887–898.

Gautam R, Vanga S, Ariese F, Umapathy S. 2015. Review of multidimensional data processing approaches for Raman and infrared spectroscopy. EPJ Techniques and Instrumentation **2**, doi.org/10.1140/epjti/s40485-015-0018-6.

De Gelder J, De Gussem K, Vandenabeele P, Moens L. 2007. Reference database of Raman spectra of biological molecules. Journal of Raman Spectroscopy **38**, 1133–1147.

Giannoutsou E, Sotiriou P, Apostolakos P, Galatis B. 2013. Early local differentiation of the cell wall matrix defines the contact sites in lobed mesophyll cells of Zea mays. Annals of Botany **112**, 1067–1081.

Gierlinger N. 2018. New insights into plant cell walls by vibrational microspectroscopy. APPLIED SPECTROSCOPY REVIEWS **53**, 517–551.

Gierlinger N, Keplinger T, Harrington M, Schwanninger M. 2013. Raman Imaging of Lignocellulosic Feedstock. In: van de Ven T, In: Kadla J, eds. Cellulose - Biomass Conversion. IntechOpen, DOI: 10.5772/50878.

Gierlinger N, Schwanninger M. 2007. The potential of Raman microscopy and Raman imaging in plant research. Spectroscopy-An International Journal **21**, 69–89.

Glynn JM, Froehlich JE, Osteryoung KW. 2008. Arabidopsis ARC6 Coordinates the Division Machineries of the Inner and Outer Chloroplast Membranes through Interaction with PDV2 in the Intermembrane Space. the Plant Cell Online **20**, 2460–2470.

Goff KL, Quaroni L, Wilson KE. 2009. Measurement of metabolite formation in single living cells of *Chlamydomonas reinhardtii* using synchrotron Fourier-Transform Infrared spectromicroscopy. Analyst **134**, 2216–2219.

Gomes da Costa S, Richter A, Schmidt U, Breuninger S, Hollricher O. 2019. Confocal Raman microscopy in life sciences. Morphologie **103**, 11–16.

Govaerts YM, Jacquemoud S, Verstraete MM, Ustin SL. 1996. Three-dimensional radiation transfer modeling in a dicotyledon leaf. Applied Optics **35**, 6585.

Graham LE, Kodner RB, Fisher MM, Graham JM, Wilcox LW, Hackney JM, Obst J, Bilkey PC, Hanson DT, Cook ME. 2004. Early land plant adaptations to terrestrial stress: A focus on phenolics. In: Hemsley AR, Poole IB, eds. The Evolution of Plant Physiology. Oxford: Academic Press, 155–169.

Gray SB, Brady SM. 2016. Plant developmental responses to climate change. Developmental Biology **419**, 64–77.

Grew N. 1682. *The anatomy of plants with an idea of a philosophical history of plants, and several other lectures, read before the royal society*. London: W. Rawlins.

Hanba YT, Miyazawa SI, Kogami H, Terashima I. 2001. Effects of leaf age on internal CO_2 transfer conductance and photosynthesis in tree species having different types of shoot phenology. Australian Journal of Plant Physiology **28**, 1075–1084.

Hanson DT, Collins AM, Jones HDT, Roesgen J, Lopez-Nieves S, Timlin JA. 2014. On-line stable isotope gas exchange reveals an inducible but leaky carbon concentrating mechanism in Nannochloropsis salina. Photosynthesis Research **121**, 311–322.

Hanson MR, Kohler RH. 2001. GFP imaging: methodology and application to investigate cellular compartmentation in plants. Journal of Experimental Botany **52**, 529–539.

Harwood R, Goodman E, Gudmundsdottir M, Huynh M, Musulin Q, Song M, Barbour MM. 2020. Cell and chloroplast anatomical features are poorly estimated from 2D cross-sections. New Phytologist **225**, 2567–2578.

Hasegawa J, Sakamoto Y, Nakagami S, Aida M, Sawa S, Matsunaga S. 2016. Three-dimensional imaging of plant organs using a simple and rapid transparency technique. Plant and Cell Physiology **57**, 462–472.

Hashimoto K, Badarla VR, Kawai A, Ideguchi T. 2019. Complementary vibrational spectroscopy. Nature Communications **10**, 1–6.

Hatakeyama Y, Ueno O. 2016. Intracellular position of mitochondria and chloroplasts in bundle sheath and mesophyll cells of C_3 grasses in relation to photorespiratory CO_2 loss. Plant Production Science **1008**, 1–12.

Hatch MD, Slack CR. 1966. Photosynthesis by sugar-cane leaves. A new carboxylation reaction and the pathway of sugar formation. The Biochemical journal **101**, 103–111.

Heinrich L, Bennett D, Ackerman D, *et al.* 2021. Whole-cell organelle segmentation in volume electron microscopy. Nature **599**, 141–146.

Heraud P, Cowan MF, Marzec KM, Møller BL, Blomstedt CK, Gleadow R. 2018. Label-free Raman hyperspectral imaging analysis localizes the cyanogenic glucoside dhurrin to the cytoplasm in sorghum cells. Scientific reports **8**, 2691.

Higa T, Suetsugu N, Wada M. 2014. Plant nuclear photorelocation movement. Journal of Experimental Botany **65**, 2873–2881.

Higashi-Fujime S. 1980. Active movement in vitro of bundles of microfilaments isolated from Nitella

cell. Journal of Cell Biology **87**, 569–578.

Ho QT, Berghuijs HNC, Watté R, *et al.* 2016. Three-dimensional microscale modelling of CO_2 transport and light propagation in tomato leaves enlightens photosynthesis. Plant Cell and Environment **39**, 50–61.

Holman H-YN, Bjornstad K, McNamara MP, Martin MC, McKinney WR, Blakely EA. 2002. Synchrotron infrared spectromicroscopy as a novel bioanalytical microprobe for individual living cells: cytotoxicity considerations. Journal of Biomedical Optics **7**, 417–424.

Hu J, Baker A Fau - Bartel B, Bartel B Fau - Linka N, Linka N Fau - Mullen RT, Mullen Rt Fau - Reumann S, Reumann S Fau - Zolman BK, Zolman BK, Plant C. 2012. Plant peroxisomes: biogenesis and function. Plant Cell **24**, 2279–2303.

Iermak I, Vink J, Bader AN, Wientjes E, Van Amerongen H. 2016. Visualizing heterogeneity of photosynthetic properties of plant leaves with two-photon fluorescence lifetime imaging microscopy. Biochimica et Biophysica Acta - Bioenergetics **1857**, 1473–1478.

Islam MS, Niwa Y, Takagi S. 2009. Light-dependent intracellular positioning of mitochondria in arabidopsis thaliana mesophyll cells. Plant and Cell Physiology **50**, 1032–1040.

Ivanova LA, Pyankov VI. 2002. Structural Adaptation of the Leaf Mesophyll to Shading. **49**, 419–431.

Iwai M, Roth MS, Niyogi KK. 2018. Subdiffraction-resolution live-cell imaging for visualizing thylakoid membranes. Plant Journal **96**, 233–243.

Jacquemoud S, Frangi J-P. 1997. Three dimensional representation of leaf anatomy–application of photon transport. Physical Measurements & Signatures in Remote Sensing **35**, 295–302.

Jacques SL. 2013. Optical properties of biological tissues: A review. Physics in Medicine and Biology **58**.

Jamme F, Vindigni JD, Méchin V, Cherifi T, Chardot T, Froissard M. 2013. Single cell synchrotron FT-IR microspectroscopy reveals a link between neutral lipid and storage carbohydrate fluxes in S. cerevisiae. PloS one **8**, 1–14.

Jiang CD, Wang X, Gao HY, Shi L, Chow WS. 2011. Systemic Regulation of Leaf Anatomical Structure, Photosynthetic Performance, and High-Light Tolerance in Sorghum. Plant Physiol **155**, 1416–1424.

Jin X, Jiang Z, Zhang K, *et al.* 2018. Three-dimensional analysis of chloroplast structures associated with virus infection. Plant Physiology **176**, 282–294.

Johnson MP, Goral TK, Duffy CDP, Brain APR, Mullineaux CW, Ruban A V. 2011. Photoprotective energy dissipation involves the reorganization of photosystem II light-harvesting complexes in the grana membranes of spinach chloroplasts. Plant Cell **23**, 1468–1479.

Kalve S, Fotschki J, Beeckman T, Vissenberg K, Beemster GTS. 2014. Three-dimensional patterns of cell division and expansion throughout the development of Arabidopsis thaliana leaves. Journal of Experimental Botany **65**, 6385–6397.

Karabourniotis G, Bornman JF, Nikolopoulos D. 2000. A possible optical role of the bundle sheath extensions of the heterobaric leaves of Vitis vinifera and Quercus coccifera. Plant, Cell and Environment **23**, 423–430.

Kasahara M, Kagawa T, Olkawa K, Suetsugu N, Miyao M, Wada M. 2002. Chloroplast avoidance movement reduces photodamage in plants. Nature **420**, 829–832.

Kaul RB. 1976. Anatomical observations on floating leaves. Aquatic Botany **2**, 215–234.

Khoshravesh R, Lundsgaard-Nielsen V, Sultmanis S, Sage TL. 2017. Light Microscopy, Transmission Electron Microscopy, and Immunohistochemistry Protocols for Studying Photorespiration. In: Fernie AR, Bauwe H, In: Weber APM, eds. Photorespiration: Methods and Protocols. New York, NY: Springer New York, 243–270.

Khoshravesh R, Stata M, Busch FA, *et al.* 2020. The Evolutionary Origin of C_4 Photosynthesis in the Grass Subtribe Neurachninae. Plant physiology **182**, 566–583.

Khoshravesh R, Stinson CR, Stata M, Busch FA, Sage RF, Ludwig M, Sage TL. 2016. C_3-C_4 intermediacy in grasses: Organelle enrichment and distribution, glycine decarboxylase expression, and the rise of C_2 photosynthesis. Journal of Experimental Botany **67**, 3065–3078.

Kirchhoff H. 2019. Chloroplast ultrastructure in plants. New Phytologist **223**, 565–574.

Kizilyaprak C, Stierhof Y-D, Humbel BM. 2019. Volume microscopy in biology: FIB-SEM tomography. Tissue and Cell **57**, 123–128.

Koch M, Zagermann S, Kniggendorf A-K, Meinhardt-Wollweber M, Roth B. 2017. Violaxanthin cycle kinetics analysed in vivo with resonance Raman spectroscopy. Journal of Raman spectroscopy: JRS **48**, 686–691.

Kodama Y. 2016. Time gating of chloroplast autofluorescence allows clearer fluorescence imaging in planta. PLoS ONE **11**, 1–8.

Kopittke PM, de Jonge MD, Wang P, *et al.* 2014. Laterally resolved speciation of arsenic in roots of wheat and rice using fluorescence-XANES imaging. New Phytologist **201**, 1251–1262.

Kopittke PM, Punshon T, Paterson DJ, Tappero R V., Wang P, Pax F, van der Ent A, Lombi E. 2018. Synchrotron-based X-ray fluorescence microscopy as a technique for imaging of elements in plants. Plant Physiology **178**, 507–523.

Krafft C, Cervellati C, Paetz C, Schneider B, Popp J. 2012. Distribution of Amygdalin in Apricot (Prunus armeniaca) Seeds Studied by Raman Microscopic Imaging. Applied Spectroscopy **66**, 644–649.

Krähmer A, Gudi G, Weiher N, Gierus M, Schütze W, Schulz H. 2013. Characterization and quantification of secondary metabolite profiles in leaves of red and white clover species by NIR and

ATR-IR spectroscopy. Vibrational Spectroscopy **68**, 96–103.

Kramer M, Rodriguez-heredia M, Saccon F, Mosebach L, Twachtmann M, Krieger-liszkay A, Duffy C, Knell RJ, Finazzi G, Hanke GT. 2021. Regulation of photosynthetic electron flow on dark to light transition by ferredoxin: NADP(H) oxidoreductase interactions. eLife **10: e56088**, doi: 10.7554/eLife.56088.

Kremer C, Pettolino F, Bacic A, Drinnan A. 2004. Distribution of cell wall components in *Sphagnum* hyaline cells and in liverwort and hornwort elaters. Planta **219**, 1023–1035.

Kurihara D, Mizuta Y, Sato Y, Higashiyama T. 2015. ClearSee: A rapid optical clearing reagent for whole-plant fluorescence imaging. Development (Cambridge) **142**, 4168–4179.

Lasch P, Kneipp J. 2008. *Biomedical Vibrational Spectroscopy*. Hoboken, N.J.: Wiley-Interscience.

Leegood RC. 2013. Strategies for engineering C_4 photosynthesis. Journal of Plant Physiology **170**, 378–388.

Lei R, Jiang H, Hu F, Yan J, Zhu S. 2017. Chlorophyll fluorescence lifetime imaging provides new insight into the chlorosis induced by plant virus infection. Plant Cell Reports **36**, 327–341.

Li M, Huang WE, Gibson CM, Fowler PW, Jousset A. 2013. Stable isotope probing and Raman spectroscopy for monitoring carbon flow in a food chain and revealing metabolic pathway. Analytical Chemistry **85**, 1642–1649.

Li L, Ma Z, Niinemets Ü, Guo D. 2017. Three key sub-leaf modules and the diversity of leaf designs. Frontiers in Plant Science **8**, 1–8.

Li Z, Wakao S, Fischer BB, Niyogi KK. 2009. Sensing and responding to excess light. Annual Review of Plant Biology **60**, 239–260.

Li L, Zhang Q, Huang D. 2014. A review of imaging techniques for plant phenotyping. Sensors

(Switzerland) **14**, 20078–20111.

Lichtenberg M, Trampe ECL, Vogelmann TC, Kühl M. 2017. Light sheet microscopy imaging of light absorption and photosynthesis distribution in plant tissue. Plant Physiology **175**, 721–733.

Ligrone R, Carafa A, Duckett JG, Renzaglia KS, Ruel K. 2008. Immunocytochemical detection of lignin-related epitopes in cell walls in bryophytes and the charalean alga Nitella. Plant Systematics and Evolution **270**, 257–272.

Longstreth DJ, Hartsock T, Nobel PS. 1980. Mesophyll cell properties for some C_3 and C_4 species with high photosynthetic rates. Physiologia Plantarum **48**, 494–498.

Louie KB, Bowen BP, McAlhany S, Huang Y, Price JC, Mao JH, Hellerstein M, Northen TR. 2013. Mass spectrometry imaging for in situ kinetic histochemistry. Scientific Reports **3**, 1–7.

Lundgren MR. 2020. C2 photosynthesis: a promising route towards crop improvement? New Phytologist **228**, 1734–1740.

Lundgren MR, Fleming AJ. 2020. Cellular perspectives for improving mesophyll conductance. Plant Journal **101**, 845–857.

Lundgren MR, Mathers A, Baillie AL, *et al.* 2019. Mesophyll porosity is modulated by the presence of functional stomata. Nature Communications **10**, doi.org/10.1038/s41467-019-10826-5.

Maai E, Shimada S, Yamada M, Sugiyama T, Miyake H, Taniguchi M. 2011. The avoidance and aggregative movements of mesophyll chloroplasts in C_4 monocots in response to blue light and abscisic acid. Journal of Experimental Botany **62**, 3213–3221.

Mai KKK, Yeung WT, Han SY, Cai X, Hwang I, Kang BH. 2019. Electron Tomography Analysis of Thylakoid Assembly and Fission in Chloroplasts of a Single-Cell C4 plant, Bienertia sinuspersici. Scientific Reports **9**, 1–12.

Marchi S, Tognetti R, Minnocci A, Borghi M, Sebastiani L. 2008. Variation in mesophyll anatomy and photosynthetic capacity during leaf development in a deciduous mesophyte fruit tree (*Prunus persica*) and an evergreen sclerophyllous Mediterranean shrub (*Olea europaea*). Trees - Structure and Function **22**, 559–571.

Matryba P, Kaczmarek L, Gołąb J. 2019. Advances in Ex Situ Tissue Optical Clearing. Laser and Photonics Reviews **13**.

Matthaeus WJ, Schmidt J, White JD, Zechmann B. 2020. Novel perspectives on stomatal impressions: Rapid and non-invasive surface characterization of plant leaves by scanning electron microscopy. PLoS ONE **15**, 1–11.

Mazurek S, Mucciolo A, Humbel BM, Nawrath C. 2013. Transmission Fourier transform infrared microspectroscopy allows simultaneous assessment of cutin and cell-wall polysaccharides of Arabidopsis petals. Plant Journal **74**, 880–891.

McClendon JH. 1984. The Micro-Optics of Leaves. I. Patterns of Reflection from the Epidermis. American Journal of Botany **71**, 1391–1397.

McCree KJ. 1971. The action spectrum, absorptance and quantum yield of photosynthesis in crop plants. Agricultural Meteorology **9**, 191–216.

Meeßen J, Backhaus T, Brandt A, Raguse M, Böttger U, De Vera JP, De La Torre R. 2017. The effect of high-dose ionizing radiation on the isolated photobiont of the astrobiological model lichen circinaria gyrosa. Astrobiology **17**, 154–162.

Michen B, Geers C, Vanhecke D, Endes C, Rothen-Rutishauser B, Balog S, Petri-Fink A. 2015. Avoiding drying-artifacts in transmission electron microscopy: Characterizing the size and colloidal state of nanoparticles. Scientific Reports **5**, doi.org/10.1038/srep09793.

Midorikawa K, Tsuchiya K, Law SSY, Miyagi Y, Asai T, Iino T, Ozeki Y, Kodama Y, Numata K. 2020.

Cellular internalization mechanism of novel Raman probes designed for plant cells. RSC Chemical Biology **1**, 204–208.

Mishra P, Asaari MSM, Herrero-Langreo A, Lohumi S, Diezma B, Scheunders P. 2017. Close range hyperspectral imaging of plants: A review. Biosystems Engineering **164**, 49–67.

Miura D, Fujimura Y, Wariishi H. 2012. In situ metabolomic mass spectrometry imaging: Recent advances and difficulties. Journal of Proteomics **75**, 5052–5060.

Miyake H, Nishimura M, Takeoka Y. 2001. Immunogold labeling of rubisco in C_4 plant leaves for scanning electron microscopy. Plant Production Science **4**, 41–49.

Mizuta Y. 2021. Advances in Two-Photon Imaging in Plants. Plant and Cell Physiology **00**, 1–7.

Moudříková Š, Mojzeš P, Zachleder V, Pfaff C, Behrendt D, Nedbal L. 2016. Raman and fluorescence microscopy sensing energy-transducing and energy-storing structures in microalgae. Algal Research **16**, 224–232.

Moudříková Š, Sadowsky A, Metzger S, Nedbal L, Mettler-Altmann T, Mojzeš P. 2017. Quantification of Polyphosphate in Microalgae by Raman Microscopy and by a Reference Enzymatic Assay. Analytical Chemistry **89**, 12006–12013.

Müller W, Kielhorn M, Schmitt M, Popp J, Heintzmann R. 2016. Light sheet Raman micro-spectroscopy. Optica **3**, 452.

Mullineaux CW. 2004. FRAP analysis of photosynthetic membranes. Journal of Experimental Botany **55**, 1207–1211.

Musielak TJ, Slane D, Liebig C, Bayer M. 2016. A versatile optical clearing protocol for deep tissue imaging of fluorescent proteins in *Arabidopsis thaliana*. PLoS ONE **11**, 1–17.

Nakamura S, Hagihara S, Otomo K, Ishida H, Hidema J, Nemoto T, Izumi M. 2021. Autophagy

Contributes to the Quality Control of Leaf Mitochondria. Plant & cell physiology **62**, 229–247.

Nelson EA, Sage RF. 2008. Functional constraints of CAM leaf anatomy: Tight cell packing is associated with increased CAM function across a gradient of CAM expression. Journal of Experimental Botany **59**, 1841–1850.

Neumüller J. 2018. Electron tomography—a tool for ultrastructural 3D visualization in cell biology and histology. Wiener Medizinische Wochenschrift **168**, 322–329.

Nguyen HDD, Pan V, Pham C, Valdez R, Doan K, Nansen C. 2020. Night-based hyperspectral imaging to study association of horticultural crop leaf reflectance and nutrient status. Computers and Electronics in Agriculture **173**, 105458.

Nicotra AB, Leigh A, Boyce CK, Jones CS, Niklas KJ, Royer DL, Tsukaya H. 2011. The evolution and functional significance of leaf shape in the angiosperms. Functional Plant Biology **38**, 535–552.

Niinemets Ü, Díaz-Espejo A, Flexas J, Galmés J, Warren CR. 2009. Role of mesophyll diffusion conductance in constraining potential photosynthetic productivity in the field. Journal of Experimental Botany **60**, 2249–2270.

Nobel PS. 1977. Internal Leaf Area and Cellular CO2 Resistance: Photosynthetic Implications of Variations with Growth Conditions and Plant Species. Physiologia Plantarum **40**, 137–144.

Nobel PS, Hartsock TL. 1981. Development of leaf thickness for Plectranthus parviflorus – Influence of photosynthetically active radiation. Physiologia Plantarum **51**, 163–166.

Ogburn RM, Edwards EJ. 2013. Repeated origin of three-dimensional leaf venation releases constraints on the evolution of succulence in plants. Current Biology **23**, 722–726.

Oguchi R, Hikosaka K, Hirose T. 2005. Leaf anatomy as a constraint for photosynthetic acclimation: Differential responses in leaf anatomy to increasing growth irradiance among three deciduous trees. Plant, Cell and Environment **28**, 916–927.

Oldenbourg R. 2013. Polarized Light Microscopy : Principles and Practice. Cold Spring Harbor Protocols, 1023–1037.

Olmos V, Benítez L, Marro M, Loza-Alvarez P, Piña B, Tauler R, de Juan A. 2017. Relevant aspects of unmixing/resolution analysis for the interpretation of biological vibrational hyperspectral images. TrAC - Trends in Analytical Chemistry **94**, 130–140.

Onoda Y, Wright IJ, Evans JR, Hikosaka K, Kitajima K, Niinemets Ü, Poorter H, Tosens T, Westoby M. 2017. Physiological and structural tradeoffs underlying the leaf economics spectrum. New Phytologist **214**, 1395–1397.

Orr DJ, Pereira AM, da Fonseca Pereira P, Pereira-Lima ÍA, Zsögön A, Araújo WL. 2017. Engineering photosynthesis: Progress and perspectives. F1000Research **6**, 1–11.

Ovec M, Komis G, Olga S. 2015. Super-resolution Microscopy in Plant Cell Imaging. Trends in Plant Science **20**, 834–843.

Ovecka M, Vaškebová L, Komis G, Luptoviak I, Smertenko A, Šamaj J. 2015. Preparation of plants for developmental and cellular imaging by light-sheet microscopy. Nature Protocols **10**, 1234–1247.

Ovečka M, von Wangenheim D, Tomančák P, Šamajová O, Komis G, Šamaj J. 2018. Multiscale imaging of plant development by light-sheet fluorescence microscopy. Nature Plants **4**, 639–650.

Palit S, Sharma A, Talukder G. 1994. Effects of Cobalt on Plants. Botanical Review **60**, 149–181.

Palmer WM, Martin AP, Flynn JR, Reed SL, White RG, Furbank RT, Grof CPL. 2015. PEA-CLARITY: 3D molecular imaging of whole plant organs. Scientific Reports **5**, 1–6.

Panteris E, Galatis B. 2005. The morphogenesis of lobed plant cells in the mesophyll and epidermis: Organization and distinct roles of cortical microtubules and actin filaments. New Phytologist **167**, 721–732.

Parodi V, Jacchetti E, Osellame R, Cerullo G, Polli D, Raimondi MT. 2020. Nonlinear Optical Microscopy: From Fundamentals to Applications in Live Bioimaging. Frontiers in Bioengineering and Biotechnology **8**, 1174.

Paunov M, Koleva L, Vassilev A, Vangronsveld J, Goltsev V. 2018. Effects of different metals on photosynthesis: Cadmium and zinc affect chlorophyll fluorescence in durum wheat. International Journal of Molecular Sciences **19**, 787; doi.org/10.3390/ijms19030787.

Perico C, Sparkes I. 2018. Plant organelle dynamics: cytoskeletal control and membrane contact sites. New Phytologist **220**, 381–394.

Perktold A, Zellnig G, Guttenberger H, Gailhofer M. 1998. 3D Reconstruction of Chloroplasts and their Ultrastructure using Ultra-Thin-Serial-Sections. Phyton - Annales Rei Botanicae **38**, 159–165.

Peterson KM, Rychel AL, Torii KU. 2010. Out of the Mouths of Plants : The Molecular Basis of the Evolution and Diversity of Stomatal Development. The Plant Cell **22**, 296–306.

Pickering IJ, Prince RC, Salt DE, George GN. 2000. Quantitative, chemically specific imaging of selenium transformation in plants. Proceedings of the National Academy of Sciences of the United States of America **97**, 10717–10722.

Piovesan A, Vancauwenberghe V, Looverbosch T Van De, Verboven P, Nicolaï B. 2021. X-ray computed tomography for 3D plant imaging. Trends in Plant Science **26**, 1171–1185.

Popper ZA, Michel G, Hervé C, Domozych DS, Willats WGT, Tuohy MG, Kloareg B, Stengel DB. 2011. Evolution and diversity of plant cell walls: From algae to flowering plants. Annual Review of Plant Biology **62**, 567–590.

Punshon T, Ricachenevsky FK, Hindt M, Socha AL, Zuber H. 2013. Methodological approaches for using synchrotron X-ray fluorescence (SXRF) imaging as a tool in ionomics: examples from *Arabidopsis thaliana*. Metallomics: integrated biometal science **5**, 1133–1145.

Pushie MJ, Pickering IJ, Korbas M, Hackett MJ, George GN. 2014. Elemental and chemically specific x-ray fluorescence imaging of biological systems. Chemical Reviews **114**, 8499–8541.

Raliya R, Saharan V, Dimkpa C, Biswas P. 2018. Nanofertilizer for Precision and Sustainable Agriculture: Current State and Future Perspectives. Journal of Agricultural and Food Chemistry **66**, 6487–6503.

Raven JA, Evans MCW, Korb RE. 1999. The role of trace metals in photosynthetic electron transport in O_2-evolving organisms. Photosynthesis Research **60**, 111–150.

Ren T, Weraduwage SM, Sharkey TD. 2019. Prospects for enhancing leaf photosynthetic capacity by manipulating mesophyll cell morphology. Journal of Experimental Botany **70**, 1153–1165.

Renz M. 2013. Fluorescence microscopy—A historical and technical perspective. Cytometry Part A **83**, 767–779.

Riyue L, Yaxin L, Shichang L, Ying W, Kim L, Ning L, Daiying X, Qinglu Z, J. GS. 2021. Three-Dimensional Superresolution Imaging of the FtsZ Ring during Cell Division of the Cyanobacterium Prochlorococcus. mBio **8**, e00657-17.

Roig-Oliver M, Bresta P, Nadal M, Liakopoulos G, Nikolopoulos D, Karabourniotis G, Bota J, Flexas J. 2020. Cell wall composition and thickness affect mesophyll conductance to CO_2 diffusion in *Helianthus annuus* under water deprivation. Journal of Experimental Botany **71**, 7198–7209.

Rosenberger HE. 1977. Differential Interference Contrast Microscopy BT - Interpretive Techniques for Microstructural Analysis. In: McCall JL, French PM, eds. Boston, MA: Springer US, 79–104.

Rymen B, Fiorani F, Kartal F, Vandepoele K, Inze D, Beemster GTSS. 2007. Cold nights impair leaf growth and cell cycle progression in maize through transcriptional changes of cell cycle genes. Plant Physiol **143**, 1429–1438.

Ryu J, Nam H, Kim HK, Joo Y, Lee SJ, Kim KH. 2014. In Vivo Monitoring of Intracellular Chloroplast

Movements in Intact Leaves of C_4 Plants Using Two-Photon Microscopy. Microscopy Research and Technique **77**, 806–813.

Sack L, Holbrook NM. 2006. Leaf hydraulics. Annual Review of Plant Biology **57**, 361–381.

Sage RF, Khoshravesh R, Sage TL. 2014. From proto-Kranz to C_4 Kranz: building the bridge to C_4 photosynthesis. J Exp Bot **65**, 3341–3356.

Sage TL, Sage RF. 2009. The functional anatomy of rice leaves: implications for refixation of photorespiratory CO_2 and efforts to engineer C_4 photosynthesis into rice. Plant Cell Physiol **50**, 756–772.

Salt DE, Baxter I, Lahner B. 2008. Ionomics and the study of the plant ionome. Annual Review of Plant Biology **59**, 709–733.

Salzer R, Siesler HW. 2014. *Infrared and Raman Spectroscopic Imaging.* John Wiley & Sons, Incorporated.

Sandelius AS, Penel C, Auderset G, Brightman A, Millard M, Morré DJ. 1986. Isolation of highly purified fractions of plasma membrane and tonoplast from the same homogenate of soybean hypocotyls by free-flow electrophoresis. Plant physiology **81**, 177–185.

Santi PA. 2011. Light sheet fluorescence microscopy: A review. Journal of Histochemistry and Cytochemistry **59**, 129–138.

Sarret G, Schroeder WH, Marcus MA, Geoffroy N, Manceau A. 2003. Localization and speciation of Zn in mycorrhized roots by µSXRF and µEXAFS. Journal De Physique. IV : JP **107**, 1193–1196.

Scanlon MJ, Conklin PA, Strable J, Li S, Scanlon MJ. 2019. On the mechanisms of development in monocot and eudicot leaves. New Phytologist **221**, 706–724.

Schermelleh L, Ferrand A, Huser T, Eggeling C, Sauer M, Biehlmaier O, Drummen GPC. 2019. Super-

resolution microscopy demystified. Nature Cell Biology **21**, 72–84.

Schneider CA, Rasband WS, Eliceiri KW. 2012. NIH Image to ImageJ: 25 years of image analysis. Nat Meth **9**, 671–675.

Schubert V. 2017. Super-resolution Microscopy – Applications in Plant Cell Research. Frontiers in Plant Science **8**, 1–12.

Schuler ML, Mantegazza O, Weber APM. 2016. Engineering C_4 photosynthesis into C_3 chassis in the synthetic biology age. Plant Journal **87**, 51–65.

Slaton MR, Smith WK. 2002. Mesophyll architecture and cell exposure to intercellular air space in alpine, desert, and forest species. International Journal of Plant Sciences **163**, 937–948.

Slattery RA, Grennan AK, Sivaguru M, Sozzani R, Ort DR. 2016. Light sheet microscopy reveals more gradual light attenuation in light-green versus dark-green soybean leaves. Journal of Experimental Botany **67**, 4697–4709.

Smith JP, Holahan EC, Smith FC, Marrero V, Booksh KS. 2019. A novel multivariate curve resolution-alternating least squares (MCR-ALS) methodology for application in hyperspectral Raman imaging analysis. Analyst **144**, 5425–5438.

Socrates G, Socrates G. 2000. *Infrared and Raman characteristic group frequencies. Tables and charts*. Chichester: WILEY.

Sotiriou P, Giannoutsou E, Panteris E, Apostolakos P, Galatis B. 2015. Cell wall matrix polysaccharide distribution and cortical microtubule organization: Two factors controlling mesophyll cell morphogenesis in land plants. Annals of Botany **117**, 401–419.

Staehelin LA, Paolillo DJ. 2020. A brief history of how microscopic studies led to the elucidation of the 3D architecture and macromolecular organization of higher plant thylakoids. Photosynthesis Research **145**, 237–258.

Stata M, Sage TL, Hoffmann N, Covshoff S, Ka-Shu Wong G, Sage RF. 2016. Mesophyll chloroplast investment in C_3, C_4 and C_2 species of the genus *Flaveria*. Plant and Cell Physiology **57**, 904–918.

Stata M, Sage TL, Rennie TD, Khoshravesh R, Sultmanis S, Khaikin Y, Ludwig M, Sage RF. 2014. Mesophyll cells of C4 plants have fewer chloroplasts than those of closely related C3 plants. Plant Cell Environ **37**, 2587–2600.

Stelzer EHK. 2002. Beyond the diffraction limit? Nature **417**, 806–807.

Strack R. 2021. Single-objective light sheet microscopy. Nature Methods **18**, 28.

Strobl F, Schmitz A, Stelzer EHK. 2017. Improving your four-dimensional image: Traveling through a decade of light-sheet-based fluorescence microscopy research. Nature Protocols **12**, 1103–1109.

Suetsugu N, Wada M. 2005. Chloroplast Photorelocation Movement. Somatic Embryogenesis, 305–320.

Sugiura D, Terashima I, Evans JR. 2020. A decrease in mesophyll conductance by Cell-Wall thickening contributes to photosynthetic downregulation. Plant Physiology **183**, 1600–1611.

Syevertsen JP, Lloyd J, McConchie C, Kriedemann PE, Farquhar GD. 1995. On the relationship between leaf anatomy and CO2 diffusion through the mesophyll of hypostomatous leaves. Plant, Cell & Environment **18**, 149–157.

Talamond P, Verdeil JL, Conéjéro G. 2015. Secondary metabolite localization by autofluorescence in living plant cells. Molecules **20**, 5024–5037.

Tanino KK, Kobayashi S, Hyett C, *et al.* 2013. Allium fistulosum as a novel system to investigate mechanisms of freezing resistance. Physiologia Plantarum **147**, 101–111.

Tanz SK, Castleden I, Small ID, Harvey Millar A. 2013. Fluorescent protein tagging as a tool to define the subcellular distribution of proteins in plants. Frontiers in Plant Science **4**, 1–9.

Taylor AO, Craig AS. 1971. Plants Under Climatic Stress. Plant physiology **47**, 710–725.

Terashima I, Fujita T, Inoue T, Chow WS, Oguchi R. 2009. Green light drives leaf photosynthesis more efficiently than red light in strong white light: Revisiting the enigmatic question of why leaves are green. Plant and Cell Physiology **50**, 684–697.

Terashima I, Hanba YT, Tholen D, Systems P, Group B. 2011. Leaf Functional Anatomy in Relation to Photosynthesis. **155**, 108–116.

Terashima I, Inoue Y. 1984. Comparative Photosynthetic Properties of Palisade Tissue Chloroplasts and Spongy Tissue Chloroplasts of *Camellia japonica* L.: Functional Adjustment of the Photosynthetic Apparatus to Light Environment within a Leaf. Plant and Cell Physiology **25**, 555–563.

Terashima I, Inoue Y. 1985. Palisade tissue chloroplasts and spongy tissue chloroplasts in spinach: Biochemical and ultrastructural differences. Plant and Cell Physiology **26**, 63–75.

Terashima I, Yano S. 2004. Developmental process of sun and shade leaves in *Chenopodium album* L. Plant, Cell and Environment **27**, 781–793.

Thain JF. 1983. Curvature Correction Factors in the Measurement of Cell Surface Areas in Plant Tissues A. Journal of Experimental Botany **34**, 87–94.

Théroux-Rancourt G, Earles JM, Gilbert ME, Zwieniecki MA, Boyce CK, McElrone AJ, Brodersen CR. 2017. The bias of a two-dimensional view: comparing two-dimensional and three-dimensional mesophyll surface area estimates using noninvasive imaging. New Phytologist **215**, 1609–1622.

Théroux-Rancourt G, Jenkins MR, Brodersen CR, McElrone A, Forrestel EJ, Earles JM. 2020. Digitally deconstructing leaves in 3D using X-ray microcomputed tomography and machine learning. Applications in Plant Sciences **8**, 1–9.

Tholen D, Boom C, Zhu XG. 2012. Opinion: Prospects for improving photosynthesis by altering leaf anatomy. Plant Science **197**, 92–101.

Thorn K. 2016. A quick guide to light microscopy in cell biology. Molecular Biology of the Cell **27**, 219–222.

Tomás M, Flexas J, Copolovici L, Galmés J, Hallik L, Medrano H, Ribas-Carbó M, Tosens T, Vislap V, Niinemets Ü. 2013. Importance of leaf anatomy in determining mesophyll diffusion conductance to CO_2 across species: Quantitative limitations and scaling up by models. Journal of Experimental Botany **64**, 2269–2281.

Tosens T, Laanisto L. 2018. Mesophyll conductance and accurate photosynthetic carbon gain calculations. Journal of Experimental Botany **69**, 5315–5318.

Tosens T, Niinemets Ü, Vislap V, Eichelmann H, Castro Díez P. 2012*a*. Developmental changes in mesophyll diffusion conductance and photosynthetic capacity under different light and water availabilities in Populus tremula: How structure constrains function. Plant, Cell and Environment **35**, 839–856.

Tosens T, Niinemets Ü, Westoby M, Wright IJ. 2012*b*. Anatomical basis of variation in mesophyll resistance in eastern Australian sclerophylls: News of a long and winding path. Journal of Experimental Botany **63**, 5105–5119.

Türker-Kaya S, Huck CW. 2017. A review of mid-infrared and near-infrared imaging: Principles, concepts and applications in plant tissue analysis. Molecules **22**, 168; doi:10.3390/molecules22010168.

Turrell FM. 1936. The Area of the Internal Exposed Surface of Dicotyledon Leaves. American Journal of Botany **23**, 255.

Ueno O. 1998. Immunogold localization of photosynthetic enzymes in leaves of various C_4 plants, with particular reference to pyruvate orthophosphate dikinase. Journal of Experimental Botany **49**, 1637–1646.

Ustin SL, Jacquemoud S. 2020. How the Optical Properties of Leaves Modify the Absorption and Scattering of Energy and Enhance Leaf Functionality BT - Remote Sensing of Plant Biodiversity. In: Cavender-Bares J, Gamon JA, Townsend PA, eds. Cham: Springer International Publishing, 349–384.

Ustin SL, Jacquemoud S, Govaerts Y. 2001. Simulation of photon transport in a three-dimensional leaf: Implications for photosynthesis. Plant, Cell and Environment **24**, 1095–1103.

Uwada T, Huang LT, Hee PY, Usman A, Masuhara H. 2017. Size-Dependent Optical Properties of Grana Inside Chloroplast of Plant Cells. Journal of Physical Chemistry B **121**, 915–922.

Vallon O, Høyer-Hansen G, Simpson DJ. 1987. Photosystem II and cytochrome b-559 in the stroma lamellae of barley chloroplasts. Carlsberg Research Communications **52**, 405–421.

Valuchova S, Mikulkova P, Pecinkova J, Klimova J, Krumnikl M, Bainar P, Heckmann S, Tomancak P, Riha K. 2019. Imaging plant germline differentiation within Arabidopsis flower by light sheet microscopy. bioRxiv, 1–19.

Valuchova S, Mikulkova P, Pecinkova J, Klimova J, Krumnikl M, Bainar P, Heckmann S, Tomancak P, Riha K. 2020. Looking below the surface in plants. eLife **9**, 9–11.

Vaughn KC. 1987. Two Immunological Approaches to the Detection of Ribulose-1,5-Bisphosphate Carboxylase in Guard Cell Chloroplasts. Plant Physiology **84**, 188–196.

Vaverkova V, Vrana O, Adam V, Pekarek T, Jampilek J, Babula P. 2014. The Study of Naphthoquinones and Their Complexes with DNA by Using Raman Spectroscopy and Surface Enhanced Raman Spectroscopy: New Insight into Interactions of DNA with Plant Secondary Metabolites. BIOMED RESEARCH INTERNATIONAL.

Verboven P, Herremans E, Helfen L, Ho QT, Abera M, Baumbach T, Wevers M, Nicolaï BM. 2015. Synchrotron X-ray computed laminography of the three-dimensional anatomy of tomato leaves. Plant Journal **81**, 169–182.

Vermaas WFJ, Timlin JA, Jones HDT, Sinclair MB, Nieman LT, Hamad SW, Melgaard DK, Haaland DM. 2008. In vivo hyperspectral confocal fluorescence imaging to determine pigment localization and distribution in cyanobacterial cells. Proceedings of the National Academy of Sciences of the United States of America **105**, 4050–4055.

Veromann-Jürgenson L-L, Brodribb TJ, Niinemets Ü, Tosens T. 2020. Variability in the chloroplast area lining the intercellular airspace and cell walls drives mesophyll conductance in gymnosperms. Journal of Experimental Botany **71**, 4958–4971.

Veromann-Jürgenson LL, Tosens T, Laanisto L, Niinemets Ü. 2017. Extremely thick cell walls and low mesophyll conductance: Welcome to the world of ancient living! Journal of Experimental Botany **68**.

Vijayan P, Willick IR, Lahlali R, Karunakaran C, Tanino KK. 2015. Synchrotron radiation sheds fresh light on plant research: The use of powerful techniques to probe structure and composition of plants. Plant and Cell Physiology **56**, 1252–1263.

Vítek P, Veselá B, Klem K. 2020. Spatial and temporal variability of plant leaf responses cascade after PSII inhibition: Raman, chlorophyll fluorescence and infrared thermal imaging. Sensors (Switzerland) **20**.

Vogelmann TC, Evans JR. 2002. Profiles of light absorption and chlorophyll within spinach leaves from chlorophyll fluorescence. Plant, Cell and Environment **25**, 1313–1323.

Voiniciuc C, Pauly M, Usadel B. 2018. Monitoring polysaccharide dynamics in the plant cell wall. Plant Physiology **176**, 2590–2600.

Wada M, Kagawa T, Sato Y. 2003. Chloroplast Movement. Annual Review of Plant Biology **54**, 455–468.

Wang P, Khoshravesh R, Karki S, Tapia R, Balahadia CP, Bandyopadhyay A, Quick WP, Furbank R, Sage TL, Langdale JA. 2017. Re-creation of a Key Step in the Evolutionary Switch from C_3 to C_4 Leaf

Anatomy. Current Biology **27**, 3278-3287.e6.

Wang P, Liang Z, Kang BH. 2019. Electron tomography of plant organelles and the outlook for correlative microscopic approaches. New Phytologist **223**, 1756–1761.

Warming G. 2020. Plant Cell Walls Tackling Climate Change : Biotechnological Strategies to Improve Crop. , 1–26.

Warren FJ, Perston BB, Galindez-Najera SP, Edwards CH, Powell PO, Mandalari G, Campbell GM, Butterworth PJ, Ellis PR. 2015. Infrared microspectroscopic imaging of plant tissues: Spectral visualization of Triticum aestivum kernel and Arabidopsis leaf microstructure. Plant Journal **84**, 634–646.

Wei D, Chen S, Liu Q. 2015. Review of fluorescence suppression techniques in Raman spectroscopy. Applied Spectroscopy Reviews **50**, 387–406.

Weng JK, Chapple C. 2010. The origin and evolution of lignin biosynthesis. New Phytologist **187**, 273–285.

Weraduwage SM, Kim SJ, Renna L, Anozie FC, Sharkey TD, Brandizzi F. 2016. Pectin methylesterification impacts the relationship between photosynthesis and plant growth. Plant Physiology **171**, 833–848.

Weston DJ, Turetsky MR, Johnson MG, *et al.* 2017. The *Sphagnome* Project: enabling ecological and evolutionary insights through a genus-level sequencing project. New Phytologist **217**, 16–25.

Wetzel DL, Eilert AJ, Pietrzak LN, Miller SS, Sweat JA. 1998. Ultraspatially-resolved synchrotron infrared microspectroscopy of plant tissue in situ. Cellular and molecular biology (Noisy-le-Grand, France) **44**, 145–168.

Wetzel DL, Srivarin P, Finney JR. 2003. Revealing protein infrared spectral detail in a heterogeneous matrix dominated by starch. Vibrational Spectroscopy **31**, 109–114.

Wiercigroch E, Szafraniec E, Czamara K, Pacia MZ, Majzner K, Kochan K, Kaczor A, Baranska M, Malek K. 2017. Raman and infrared spectroscopy of carbohydrates: A review. Spectrochimica Acta - Part A: Molecular and Biomolecular Spectroscopy **185**, 317–335.

Wilson S, Ruban A V. 2020. Rethinking the Influence of Chloroplast Movements on Non-photochemical Quenching and Photoprotection. Plant physiology **183**, 1213–1223.

Wu Y, Gong W, Yang W. 2017. Shade Inhibits Leaf Size by Controlling Cell Proliferation and Enlargement in Soybean. Scientific Reports **7**, 1–10.

Wuyts N, Palauqui J-C, Conejero G, Verdeil J-L, Granier C, Massonnet C. 2010. High-contrast three-dimensional imaging of the Arabidopsis leaf enables the analysis of cell dimensions in the epidermis and mesophyll. Plant Methods **6**, doi.org/10.1186/1746-4811-6-17.

Xiao Y, Tholen D, Zhu X. 2016. The influence of leaf anatomy on the internal light environment and photosynthetic electron transport rate: exploration with a new leaf ray tracing model. Journal of Experimental Botany **67 (21)**, 6021–6035.

Xie J, Fernandes SB, Mayfield-Jones D, Erice G, Choi M, Lipka AE, Leakey ADB. 2021. Optical topometry and machine learning to rapidly phenotype stomatal patterning traits for maize QTL mapping. Plant Physiology.

Xin H, Zhang X, Yu P. 2013. Using synchrotron radiation-based infrared microspectroscopy to reveal microchemical structure characterization: frost damaged wheat vs. normal wheat. International journal of molecular sciences **14**, 16706–16718.

Yamada M, Kawasaki M, Sugiyama T, Miyake H, Taniguchi M. 2009. Differential positioning of C_4 mesophyll and bundle sheath chloroplasts: Aggregative movement of C_4 mesophyll chloroplasts in response to environmental stresses. Plant and Cell Physiology **50**, 1736–1749.

Yamane K, Oi T, Enomoto S, Nakao T, Arai S, Miyake H, Taniguchi M. 2018. Three-dimensional

ultrastructure of chloroplast pockets formed under salinity stress. Plant Cell and Environment **41**, 563–575.

Yang S, Li B, Slipchenko MN, Akkus A, Singer NG, Yeni YN, Akkus O. 2013. Laser Wavelength Dependence of Background Fluorescence in Raman Spectroscopic Analysis of Synovial Fluid from Symptomatic Joints. Journal of Raman spectroscopy : JRS **44**, 1089–1095.

Yang Y, Wang X, Zhao C, Tian G, Zhang H, Xiao H, He L, Zheng J. 2017. Chemical Mapping of Essential Oils, Flavonoids and Carotenoids in Citrus Peels by Raman Microscopy. Journal of food scince **82**, 2840–2846.

Yoder DW, Kadirjan-Kalbach D, Olson BJSC, Miyagishima SY, Deblasio SL, Hangarter RP, Osteryoung KW. 2007. Effects of mutations in Arabidopsis FtsZ1 on plastid division, FtsZ ring formation and positioning, and FtsZ filament morphology in vivo. Plant and Cell Physiology **48**, 775–791.

Yun MJ, Sim YH, Cha SI, Lee DY. 2019. Leaf Anatomy and 3-D Structure Mimic to Solar Cells with light trapping and 3-D arrayed submodule for Enhanced Electricity Production. Scientific Reports **9**, 1–9.

Zernike F. 1955. How I discovered phase contrast. Science **121**, 345–349.

Zhang Y, Huang T, Jorgens DM, Nickerson A, Lin LJ, Pelz J, Gray JW, López CS, Nan X. 2017. Quantitating morphological changes in biological samples during scanning electron microscopy sample preparation with correlative super-resolution microscopy. PLoS ONE **12**, 1–15.

Zhao Y, Man Y, Wen J, Guo Y, Lin J. 2019. Advances in Imaging Plant Cell Walls. Trends in Plant Science **24**, 867–878.

Zhen S, Bugbee B. 2020. Far-red photons have equivalent efficiency to traditional photosynthetic photons: Implications for redefining photosynthetically active radiation. Plant Cell and Environment

43, 1259–1272.

Zhu N, Wu D, Chen K. 2018. Label-free visualization of fruit lignification: Raman molecular imaging of loquat lignified cells. Plant Methods **14**, 1–16.

Zhu G, Zhu X, Fan Q, Wan X. 2011. Raman spectra of amino acids and their aqueous solutions. Spectrochimica Acta - Part A: Molecular and Biomolecular Spectroscopy **78**, 1187–1195.

Ziemienowicz A. 2014. Agrobacterium-mediated plant transformation: Factors, applications and recent advances. Biocatalysis and Agricultural Biotechnology **3**, 95–102.

Zwieniecki MA, Boyce CK. 2014. Evolution of a unique anatomical precision in angiosperm leaf venation lifts constraints on vascular plant ecology. Proceedings of the Royal Society B: Biological Sciences **281**, 1–7.

Tables

Table 1: A summary of microscopy imaging techniques that have been applied in photosynthesis research.

The advantage and limitations listed here are about leaf and/or photosynthetic cell structure and may not apply to all cell and tissue types. The examples listed in the table aim to represent the application of each technique, not to provide a full list of the research in the relative field. We appreciate the value of all the works that have not been cited here.

Technique	Advantages	Limitations	Representative application in photosynthesis research
Optical microscopy[1]			
Light Microscopy			
Bright-field light microscopy White light passes through the sample and the image is a result of the intensity of light transmitted or absorbed by the sample. See Cisek *et al.,* (2009) for a comprehensive review.	• Simple to use and easily available • The contrast could be improved by sectioning and staining • Suitable for live single-cell imaging • Suitable for imaging cells with natural contrast such as chloroplast containing plant cells	• Low resolution for subcellular components if not stained or pigmented • Low magnification • Low contrast with live cells • Lack of depth • Sectioning adds contrast to the thick sections such as leaves but because the tissue is delicate, infiltration in hard medium and dehydration is required	Widely used to • Characterize general leaf anatomy, stomata morphology, and density (Bolhàr-Nordenkampf and Draxler, 1993) • Identify cell and organelle arrangement in diverse photosynthetic types e.g. Kranz anatomy in C_4 species (Edwards and Voznesenskaya, 2011) • Understand the role of leaf anatomy in mesophyll conductance to CO_2 (Evans and Von Caemmerer, 1996; Evans, 2020)
Darkfield illumination Light passes through a disk which blocks the central light allowing the peripheral light to pass through the sample.	• Improved contrast • Suitable for live imaging	• Higher contrast could lead to optical artifacts • Not suitable for stained cells and tissue • Low resolution for subcellular	• Visualize chloroplasts in live cells (Higashi-Fujime, 1980; Uwada *et al.,* 2017)

components

Phase-contrast light microscopy[2]

A ring of light illuminates the specimen. The background and scattered light in the region of the specimen interfere in a way that increases the contrast (Zernike, 1955)	• Improved contrast • Suitable for single-cell live imaging	• Not suitable for stained cells and tissue • Dyes and markers are not detected • Low resolution for subcellular components	• Visualize chloroplasts in live cells (Higashi-Fujime, 1980)

Polarized light microscopy[2]

Polarized light is used to enhance contrast. For technical details see Oldenbourg *et al.,* (2013)	• Detect birefringent objects such as starch granules in a natural state • Suitable for transparent single-cell live imaging such as algae	• Dyes and markers are not detected; not suitable for stained samples • Low resolution for subcellular components	• Identify the arrangement of light-harvesting pigment-protein complexes in thylakoid grana (Garab *et al.,* 1988)

Differential interference or Nomarski interference contrast microscopy (DIC)

Polarized light is used to enhance contrast and depth to the specimen. For a review of the method see Rosenberger (1977).	• Suitable for transparent samples containing an object with a different refraction index, *e.g.* mesophyll cells containing chloroplasts • Enhances depth relative to bright field light microscopes	• Not suitable for stained samples • Low resolution for subcellular components	• Phenotype chloroplasts (Yoder *et al.,* 2007; Glynn *et al.,* 2008; Wang *et al.,* 2017)

Fluorescent based optical microscopy

Epifluorescence microscopy

Specific illuminating wavelength passes through the objective and excites the tissue. The same objective collects the emission then the emitted light passes through wavelength-specific filters and to the oculars of the camera.	• Fast and easy • Works well with thinly sectioned specimens • Provide direct observation of the samples via oculars	• Emission from the out of focus region creates background noise • High cross-talk between different channels • Lack of depth • General limitations for fluorescent-based microscopy of leaves such as optical	• Profile the distribution of photosynthetic pigments inside the leaf (Vogelmann and Evans, 2002; Borsuk and Brodersen, 2019)

		heterogeneity and chlorophyll autofluorescence	
Laser scanning and hyperspectral[3] confocal fluorescent microscopy			
Optical sectioning of the tissue is enabled by using a pinhole that blocks and eliminates the emission from out-of-focus regions. The confocal imaging method could be coupled with other technologies such as Raman micro-spectroscopy to eliminate out-of-focus signals.	• Increased signal-to-noise relative to epifluorescent microscopes • Reduces cross-talk between channels • Images up to >100 µm of tissue depth depending on the specimen optical density	• Long acquisition time • Potential photobleaching and phototoxicity due to long acquisitions • General limitations for fluorescent-based microscopy of leaves such as optical heterogeneity and chlorophyll autofluorescence	• Widely applied to detect endogenous and exogenous fluorophores inside the leaf • Assess fluorescence recovery of chloroplasts after photobleaching (Mullineaux, 2004) • Characterize inner membrane dynamics and reorganization of chloroplasts in live cells (Johnson *et al.,* 2011) • Identify the subcellular distribution of photosynthetic pigments using hyperspectral confocal microscopy (Vermaas *et al.,* 2008; Hanson *et al.,* 2014)
Light-sheet fluorescent microscopes			
Optical sectioning of the tissue is enabled by illumination and excitation of a thin layer instead of the entire specimen (Santi, 2011; Strobl *et al.,* 2017).	• High signal-to-noise ratio and resolution relative to laser scanning confocal microscopy • Increased speed of imaging relative to laser scanning confocal microscopy • Reduced tissue damage and photobleaching • Higher depth of imaging	• Specific sample preparation required • Small sample holders cannot accommodate larger samples of leaf • General limitations for fluorescent-based microscopy of leaves such as optical heterogeneity and chlorophyll autofluorescence	• Measure chlorophyll fluorescence (Lichtenberg *et al.,* 2017) • Determine the light behavior inside leaf tissue (Slattery *et al.,* 2016)
Spinning disk confocal microscopy			
Improved illumination and multi-point scanning (vs. single-point	• Reduced photobleaching and phototoxicity due to faster	• A smaller field of view relative to laser scanning confocal	• Assess organelle dynamics in response to stressors (Nakamura

scanning in laser scanning confocal microscopy) is enabled by placing multiple pinholes on a spinning disk.	acquisition time • Higher special resolution relative to laser scanning confocal microscopy • Great temporal resolution due to higher number of frames per scanning time • Very effective for high magnification imaging	microscopy • Not as effective for low magnification scanning • Less available than laser scanning confocal microscopy • General limitations for fluorescent-based microscopy of leaves such as optical heterogeneity and chlorophyll autofluorescence	*et al.,* 2021)
Fluorescence lifetime imaging (FLIM)			
Instead of the intensity of fluorescence, FLIM depends on the fluorescence lifetime of a fluorophore in different environments such as the number of de-excitation pathways, thus analyzing the cellular environment based on the molecular behavior of the fluorophore (Datta *et al.,* 2020).	• Powerful in imaging endogenous fluorophores such as photosynthetic pigments • Discriminates spectral overlap based on fluorescent lifetime • The fluorescent decay time is independent of microscope settings such as laser intensity so FLIM is more reproducible by different instrumental settings • Depth imaging is possible when a multi-photon technique is combined with FLIM	• Long acquisition time • Sensitive to changes in cellular pH and viscosity • General limitations for fluorescent-based microscopy of leaves such as optical heterogeneity and chlorophyll autofluorescence	• Reduce chloroplast autofluorescence in live imaging (Kodama, 2016) • Determine the spatial distribution and dynamics of PSI and PSII *in vivo* (Broess *et al.,* 2009; Iermak *et al.,* 2016) • Analyze *in vivo* chloroplast function based on chlorophyll fluorescence (Ryu *et al.,* 2014) • Assess viral infection effect on leaf health by measuring chlorophyll fluorescence lifetime (Lei *et al.,* 2017)
Super-resolution microscopy			
Embraces a variety of techniques that have been developed to overcome Abbe diffraction limit (~200 nm) in optical microscopy by methods ranging from localizing single molecule to structured and patterned illumination coupled with sophisticated image analysis	• Achieves as high as 10 nm lateral resolution in live-cell imaging that fills the resolution gap between confocal live imaging and destructive EM practices • Powerful visualization of ultracellular structure and molecular interaction	• General limitations for fluorescent-based microscopy of leaves such as optical heterogeneity and chlorophyll autofluorescence • Labeling barriers of leaf tissue may imposes could limit the application of Super-Resolution	• Structured Illumination Microscopy (SIM) was used to visualize thylakoid organization and dynamics (Iwai *et al.,* 2018), endoplasmic reticulum running through plasmodesmata that connects parenchyma cells in tobacco leaves (Fitzgibbon *et al.,*

(Schermelleh *et al.,* 2019)		Single-Molecule Localization Microscopy	2010) and FtsZ ring – which is also involved in plants chloroplast division - during cell division in cyanobacteria (Riyue *et al.,* 2021).
Two-(multi)photon microscopy			
The energy of one short-wavelength photon (*e.g.* 400 nm) is divided into two long-wavelength photons (*e.g.* 800 nm each) which are absorbed negligibly by most biological objects but can still excite them (Adur *et al.,* 2016; Parodi *et al.,* 2020)	Relative to laser scanning confocal microscopy, two-photon microscopy has • Increased depth of imaging up to 2-3 times • Reduced total photobleaching and photodamage due to lower energy wavelengths of excitation • Reduced autofluorescence • Increased resolution and contrast	• Although reduced, general limitations for fluorescent-based microscopy of leaves • Photobleaching in the focal plane may exceed the single-photon excitation photobleaching rate	• Determine the spatial distribution and dynamics of PSI and PSII *in vivo* (Broess *et al.,* 2009; Iermak *et al.,* 2016) • Detect *in vivo* chloroplast response to light (Ryu *et al.,* 2014)
Electron microscopy[4]			
Transmission Electron Microscopy (TEM)			
Electron beam transmits through a an ultra-thin layer of the tissue. The image reflects the density of the tissue as the denser parts transmit less electron beam and appear darker.	• High resolution, resolves distances up to 0.5 nm • Routine and standard protocols have been developed and tested for plant leaves	• Destructive • Heavy use of hazardous chemicals and heavy metals • Tissue processing could introduce artifact and size alteration	Widely used to • Characterize ultracellular structure and organization in photosynthetic cells (Tomás *et al.,* 2013; Stata *et al.,* 2016) • Detect structure and organization of the thylakoids (Staehelin and Paolillo, 2020) • Detect subcellular localization proteins via immunolocalization (Khoshravesh *et al.,* 2020) • Identify the density and localization of plasmodesmata (Bell and Oparka, 2011)
Scanning Electron Microscopy (SEM)			
Electron beam interacts with the surface; scattered and transmitted	• Obtains sub-nanometer	• Destructive	• Characterize leaf epidermis,

beam provides information on the topology of the object surface.	resolutions • Provides limited 3D information, *e.g.* of stomata patterning or freeze fractured leaves	• Does not preserve membranes and subcellular details • Feezing and critical point drying may cause shrinkage, size alteration, and structural deformation	stomata morphology, and density (Van Gardingen *et al.,* 1989; Matthaeus *et al.,* 2020) • Quantify plasmodesmata density in photosynthetic cells (Danila *et al.,* 2016, 2018, 2019) • View internal leaf structure in 3D (Sage and Sage, 2009) • Visualize immunogold labeling of photosynthetic enzymes inside cells (Miyake *et al.,* 2001)
Serial Block-Face Scanning Electron Microscopy (SBF-SEM)			
The face of a resin block is repeatedly sectioned by an ultramicrotome and imaged by SEM, allowing the creation of many hundreds of high-resolution 2D sample views that are used for 3D reconstruction.	• Provides high-resolution volume information on cell and tissue • Cover large fields of view that enable characterization of cell and tissue geometry simultaneous with organellar 3D reconstruction	• Similar drawbacks of tissue preparation for TEM • Time-consuming and labor-intensive due to manually segmented organelles • Manual subcellular segmentation may introduce human error and inconsistency in reproduction • Lower resolution relative to the other EM-based 3D imaging[4]	• Reconstruct ultrastructural features in 3D, evaluate morphological features, and quantify the volume of leaf cells and chloroplasts (Yamane *et al.,* 2018; Harwood *et al.,* 2020)
Focused Ion Beam Scanning Electron Microscopy (FIB-SEM)			
The ion beam removes layers from the face of a resin-embedded block and the SEM images backscattered electrons. Repeating this process allows the creation of many hundred high-resolution images from cellular and ultrastructural volume reconstruction (Kizilyaprak *et al.,* 2019).	• Provides volume information on cellular ultrastructure with the resolutions comparable to TEM • Strong in high-resolution imaging of membranes that suits the technique for chloroplast inner membrane characterization	• Similar drawbacks of tissue preparation for TEM • Manual subcellular segmentation may introduce human error and inconsistency in reproduction • The small field of view suits the method for organelle 3D evaluation and may not cover the large mesophyll cells	• Visualize chloroplast inner membranes in response to viral infection in 3D (Jin *et al.,* 2018) • Evaluate starch granules in chloroplasts (Crumpton-Taylor *et al.,* 2012)

Electron tomography			
Ultra-thin sections of the resin embedded tissue are imaged by TEM from different angles, the images are used to reconstruct the volume (Neumüller, 2018)	• Up to sub-nanometer resolution suits the method for visualization of membranes	• Similar drawbacks of tissue preparation for TEM • Manual subcellular segmentation may introduce human error and inconsistency in reproduction • Restricted volume suitable only for very small cellular ultrastructures such as thylakoids and plasmodesmata	• Characterize 3D network of chloroplast membrane organization, *e.g.* the helical arrangement of thylakoid (Bussi *et al.,* 2019; Mai *et al.,* 2019)

[1]See Cisek *et al.,* 2009 for a comprehensive review on optical microscopes

[2] The polarized and phase-contrast techniques discussed here are based on the conventional methods initially developed to complement bright-field light microscopes.

[3]Hyperspectral data collection gathers the full spectrum emitted from each pixel in an image. As a result, each optical section is a complex 3D data set containing pixels with x, y, and corresponding spectrum of wavelengths (lambda). This is in contrast to the more conventional signal detection methods that collect the intensity of the signal, or a few discrete signals (red, green, blue), to create images (Gao and Smith, 2015). Hyperspectral data collection has been integrated into a variety of techniques such as confocal and light-sheet fluorescent microscopy in the visible as well Raman and IR micro-spectroscopy.

[4]To compare EM-based 3D imaging in detail, please see Earles *et al*. (2019).

Boxes

Box 1. Tissue optical clearing

In tissue optical clearing (TOC) methods, the whole tissue is fixed in an aldehyde-based fixative and embedded in a media such as hydrogel to remove pigments. TOC enables deeper penetration inside a large volume and provides hundreds of virtual instead of microtome sectioning (Matryba *et al.,* 2019). Modern TOC methods -*e.g.* PEA-CLARITY or ClearSee- which retains the protein fluorescence signals (such as GFP) or allows immunolocalization of proteins in cleared tissue- have been developed for plant leaves (Wuyts *et al.,* 2010; Kurihara *et al.,* 2015; Palmer *et al.,* 2015). Tissue preparation for these methods could take three days to three weeks depending on the method. However, when preservation of proteins for immunolabeling is not intended, a more time-efficient TOC such as ethanol-acetic acid fixation and clearing with TDE (2,20-thiodiethanol) to 3-5 passive days with fewer and less-hazardous chemical treatments relative to resin infiltration and embedding (Hasegawa *et al.,* 2016; Musielak *et al.,* 2016). TOC stacks are homogenous (all water phase), thus not enabling the segmentation of gas and water phase as is done on micro-CT stacks. However, TOC combined with cell wall staining (Figure 3) is possible in every laboratory equipped with a laser scanning confocal or multiphoton excitation microscope. Scanning an area of 250 x 250 μm^2 with 100 µm depth, 0.49 µm lateral and 0.5 µm axial resolution is achievable in 10-15 minutes, providing hundreds of virtual sections (Figure 3) to fulfill the minimum requirement of S_m and IAS 2D estimation (Théroux-Rancourt *et al.,* 2017). Moreover, morphological segmentation algorithms available in open source applications such as ImageJ (Schneider *et al.,* 2012) enable investigation of the individual cell geometry (Figure 3G) and dimension (Wuyts *et al.,* 2010; Danila *et al.,* 2016, 2018), S_m and IAS 3D estimation, stomata and vein density, and their relationship with IAS and S_m.

Box 2. X-ray spectroscopy basics

When atoms interact with the incident X-ray, electrons of low-energy orbitals move up to the higher-level energy. To restabilize the atomic equilibrium, an atom from higher-level orbitals fills this vacancy of the low energy and emits the extra energy as X-ray fluorescence; the absorption and emission patterns being identical for each element (Dolenko *et al.,* 2017). Multiple methods of X-ray spectroscopy including X-ray fluorescence microscopy (XFM), X-ray absorption spectroscopy (XAS) have been developed which have two very basic principles in common: the absorption/emission pattern of each element is inferred as its fingerprint and the intensity of the absorption/emission represents the concentration of the element of interest enabling simultaneous localization and quantification of a specific element in a complex matrix. Synchrotron radiation-based X-ray has been used as the main source of radiation in biological X-ray spectroscopy research due to its significantly higher X-ray flux, higher time resolution (milliseconds or less), and tunability of the radiation (Lombi and Susini, 2009).

Box 3. Infrared and Raman spectroscopy basics

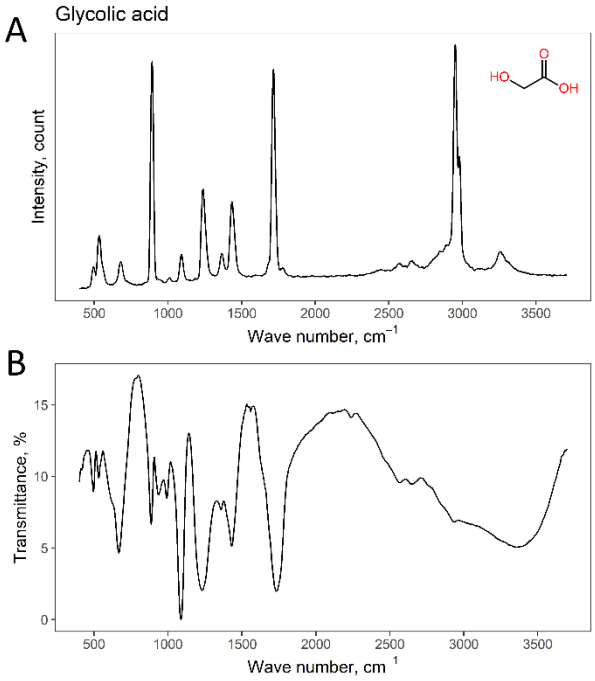

When materials are illuminated by visible or infrared light, the covalent bonds between atoms absorb the energy and based on the strength of the bond exhibit vibration in different forms from stretching to bending (Socrates and Socrates, 2000). In Raman scattering spectroscopy, the intensity of a small portion of light (inelastic light) scattered by the atomic bonds is depicted as a function of wavenumber [proportionally related to the energy of vibration; Graph A (Dietzek *et al.,* 2018)]; In IR absorption spectroscopy, the percent of IR radiation absorbed or transmitted by the atomic bonds are expressed as a function of wavenumber, Graph B (Stuart, 2015). Symmetric and asymmetric bonds behave differently when interacting with light. Usually, symmetrical bonds are Raman active and asymmetrical bonds are IR active. These characteristics make IR more efficient in detecting functional groups and Raman in detecting backbones (*e.g.* C-C bond), but some bonds are both Raman and IR active. These differences sometimes list IR and Raman spectroscopy as complementary methods that together provide a full image of the chemical structure of the molecules (Hashimoto *et al.,* 2019; Farber *et al.,* 2019), however, they are powerful when used alone. A is simulated by http://www.cheminfo.org/Spectra/IR/Exercises/Browse_Spectra/index.html and B is scanned by a WiTec alpha 330 confocal Raman microscope.

Figure legends

Figure 1: A schematic figure of a photosynthetic leaf and its relationship with the environment on different scales.

Drawing has been made from the real plants and light and electron micrographs of a sunflower leaf following the accurate scales but the abaxial epidermis is modified to represent general broad-leaf anatomy with higher stomatal density on the abaxial side. 2PG, 2-phosphoglycolate; 3PGA, 3-phosphoglycerate; G3P, Glyceraldehyde-3-Phosphate; IAS, intercellular air space; SP, spongy mesophyll; PA, palisade mesophyll; ST, stomata; VB, vascular bundle (bundle sheath cells surrounding the vascular tissue are shown as circles); *c*, chloroplast; *m*, mitochondria; *p*, peroxisome; *ct*, cytosol; *cw*, cell wall; *grt*, grana thylakoids; *stt*, stroma thylakoids; *va*, vacuole.

Figure 2: Number of publications focused on plan cell 3D imaging from 1990-2020.

The area chart represents the number, and the inset pie chart shows the percent of 252 publication records focused on plant organ's 3D cell imaging and internal anatomy from 1990-2020. The 3D plant cell research is led by root imaging (43%) and followed by leaf (26 %). The publication records were downloaded from the Web of Science using the combination of keywords: "three-dimensional" AND "organ" AND "plant" AND "imaging". The organ list included leaf, root, stem, embryo, and seed. The original 436 publications contained 195 records for leaf, 172 for root, and 55 for the stem. After removing the content focused on the 3D imaging of the full leaf/shoot/root geometry and morphology

rather than internal 3D cellular structures these numbers were reduced to 67 (leaf), 111 (root), and 34 (stem) internal anatomy.

Figure 3: Two and three-dimensional view of a rice leaf blade.

A) A 2 µm thin cross-section of rice leaf blade obtained from conventional light microscopy (Khoshravesh *et al.,* 2017) compared with a TDE cleared leaf (B-F). B) A 3D leaf reconstruction from cleared rice leaf stained with 1 % calcofluor white overnight and cleared in 97% TDE (Hasegawa *et al.,* 2016). C) a low magnification of abaxial epidermis, arrows point to stomata. D-F) virtual sections from paradermal (D), longitudinal (E), and cross-sectional (F) view of the cube presented in B. G) a 3D reconstruction of a mesophyll cell marked in F. Scale bares = 50 µm For A-F and 10 µm for G. Leaf volume imaged by Zeiss LSM 870; 250 x 250 μm^2 x 100 µm depth, lateral resolution = 0.49 µm, axial resolution = 0.5 µm.

Figure 4: A simplified example of non-destructive spatial identification of cellular components using a hyperspectral Raman image of a *Sphagnum* sp. branch leaf.

A) A paradermal image of a *Sphagnum* sp. branch leaf taken by light microscopy. B) A 3D reconstruction of the *Sphagnum* branch leaf stained with calcofluor white to detect cellulose (silver) and autofluorescence of chlorophylls to detect chloroplast, depicting hyaline and photosynthetic chlorophyllose cells. C) Raman hyperspectral image of the rectangular inset in section A, arbitrarily

colored. D) Sum of the spectra over the scanned area. E&F) Spatial mapping for the first components (C1) of the MCR-AML Analysis for the Raman spectra (E) and MCR-AML corresponding spectra (F, C1-C3). C1 spectrum shows a high concentration of cell wall components such as cellulose (peaks 1103, 1118, 1380) and lignin-like polymers (peaks 1446, 1600, which spatially corresponds with the cell walls of chlorophyllose cells and the fibrils of hyaline cells. G) Raman spectrum of commercial cellulose used as a reference here. Leaf and cellulose imaged by a WiTec alpha 330; excitation = 523 nm; Lateral resolution = 0.3 µm; spectral resolution = 2.3 cm^{-1}. Terminology for leaf cells adopted from Weston *et al.* (2017); Raman peaks were identified following Socrates and Socrates (2000) and Zhu *et al.* (2018); MCR-AML analysis has been done in Matlab Hypertools toolbox (Amigo *et al.,* 2015).

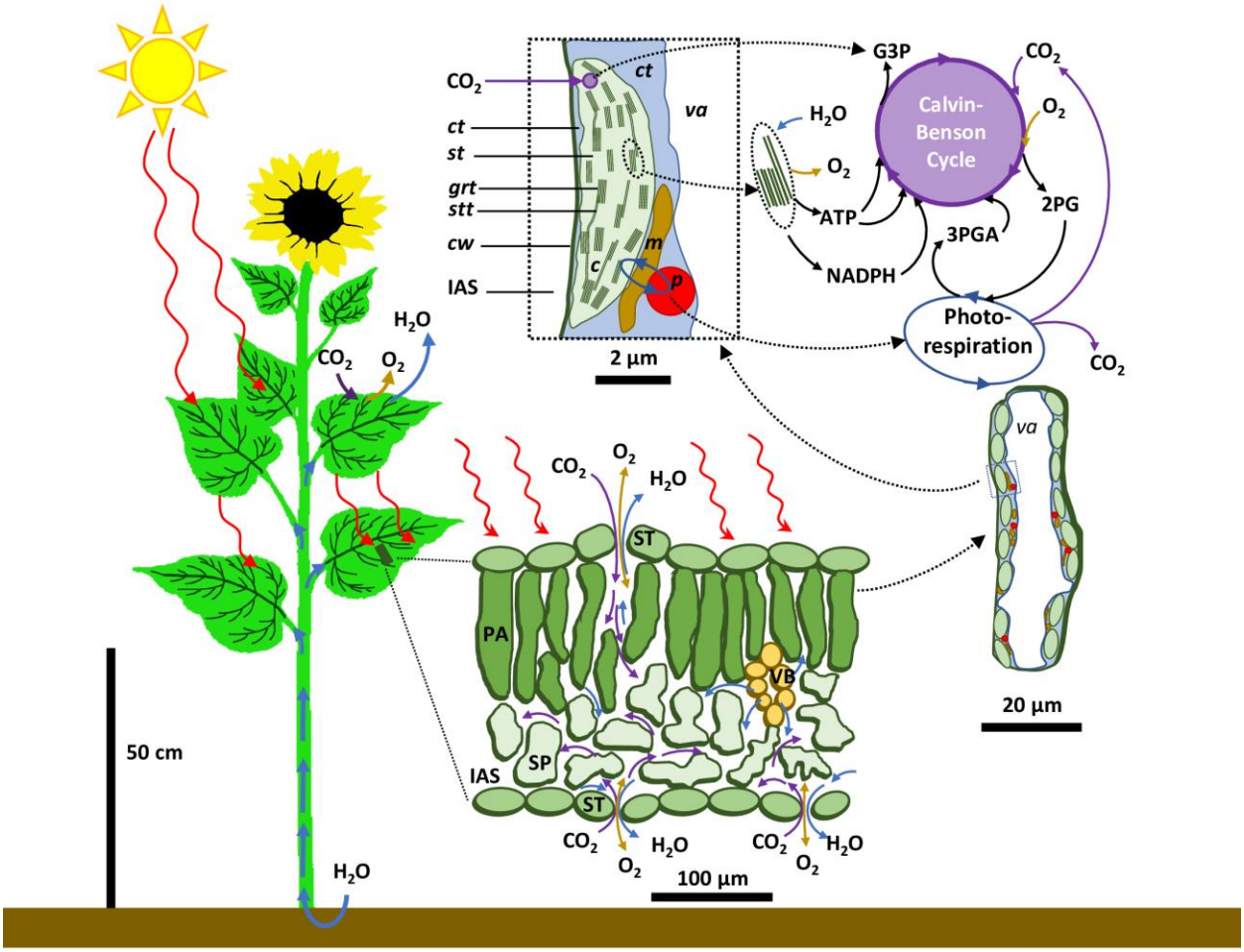

Figure 1: A schematic figure of a photosynthetic leaf and its relationship with the environment on different scales.

Drawing has been made from the real plants and light and electron micrographs of a sunflower leaf following the accurate scales but the abaxial epidermis is modified to represent general broad-leaf anatomy with higher stomatal density on the abaxial side. 2PG, 2-phosphoglycolate; 3PGA, 3-phosphoglycerate; G3P, Glyceraldehyde-3-Phosphate; IAS, intercellular air space; SP, spongy mesophyll; PA, palisade mesophyll; ST, stomata; VB, vascular bundle (bundle sheath cells surrounding the vascular tissue are shown as circles); *c*, chloroplast; *m*, mitochondria; *p*, peroxisome; *ct*, cytosol; *cw*, cell wall; *grt*, grana thylakoids; *stt*, stroma thylakoids; *va*, vacuole.

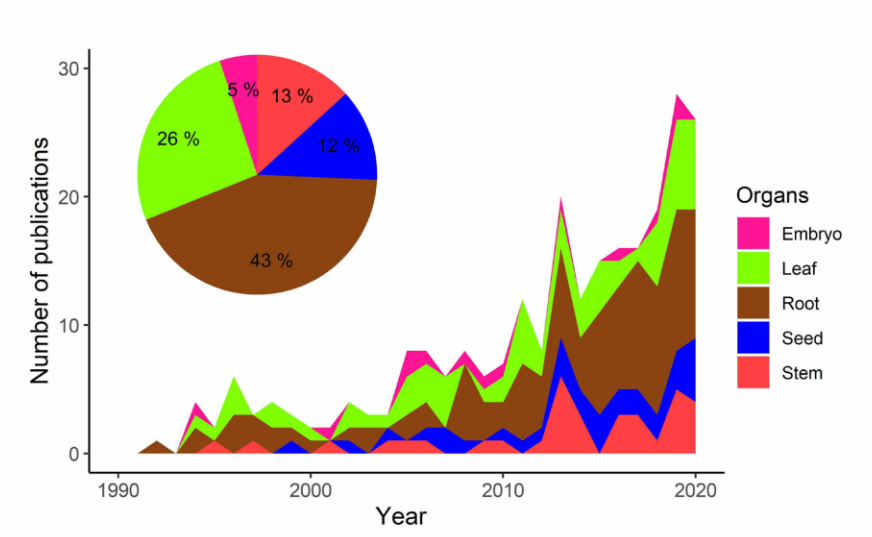

Figure 2: Number of publications focused on plan cell 3D imaging from 1990-2020.

The area chart represents the number, and the inset pie chart shows the percent of 252 publication records focused on plant organ's 3D cell imaging and internal anatomy from 1990-2020. The 3D plant cell research is led by root imaging (43%) and followed by leaf (26 %). The publication records were downloaded from the Web of Science using the combination of keywords: "three-dimensional" AND "organ" AND "plant" AND "imaging". The organ list included leaf, root, stem, embryo, and seed. The original 436 publications contained 195 records for leaf, 172 for root, and 55 for the stem. After removing the content focused on the 3D imaging of the full leaf/shoot/root geometry and morphology rather than internal 3D cellular structures these numbers were reduced to 67 (leaf), 111 (root), and 34 (stem) internal anatomy.

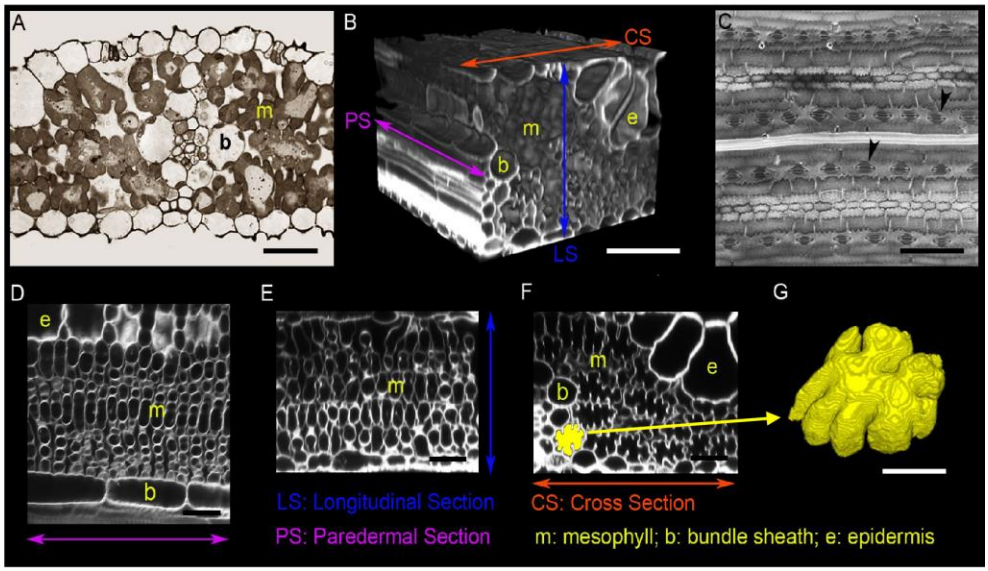

Figure 3: Two and three-dimensional view of a rice leaf blade.

A) A 2 µm thin cross-section of rice leaf blade obtained from conventional light microscopy (Khoshravesh *et al.,* 2017) compared with a TDE cleared leaf (B-F). B) A 3D leaf reconstruction from cleared rice leaf stained with 1 % calcofluor white overnight and cleared in 97% TDE (Hasegawa *et al.,* 2016). C) a low magnification of abaxial epidermis, arrows point to stomata. D-F) virtual sections from paradermal (D), longitudinal (E), and cross-sectional (F) view of the cube presented in B. G) a 3D reconstruction of a mesophyll cell marked in F. Scale bares = 50 µm For A-F and 10 µm for G. Leaf volume imaged by Zeiss LSM 870; 250 x 250 μm^2 x 100 µm depth, lateral resolution = 0.49 µm, axial resolution = 0.5 µm.

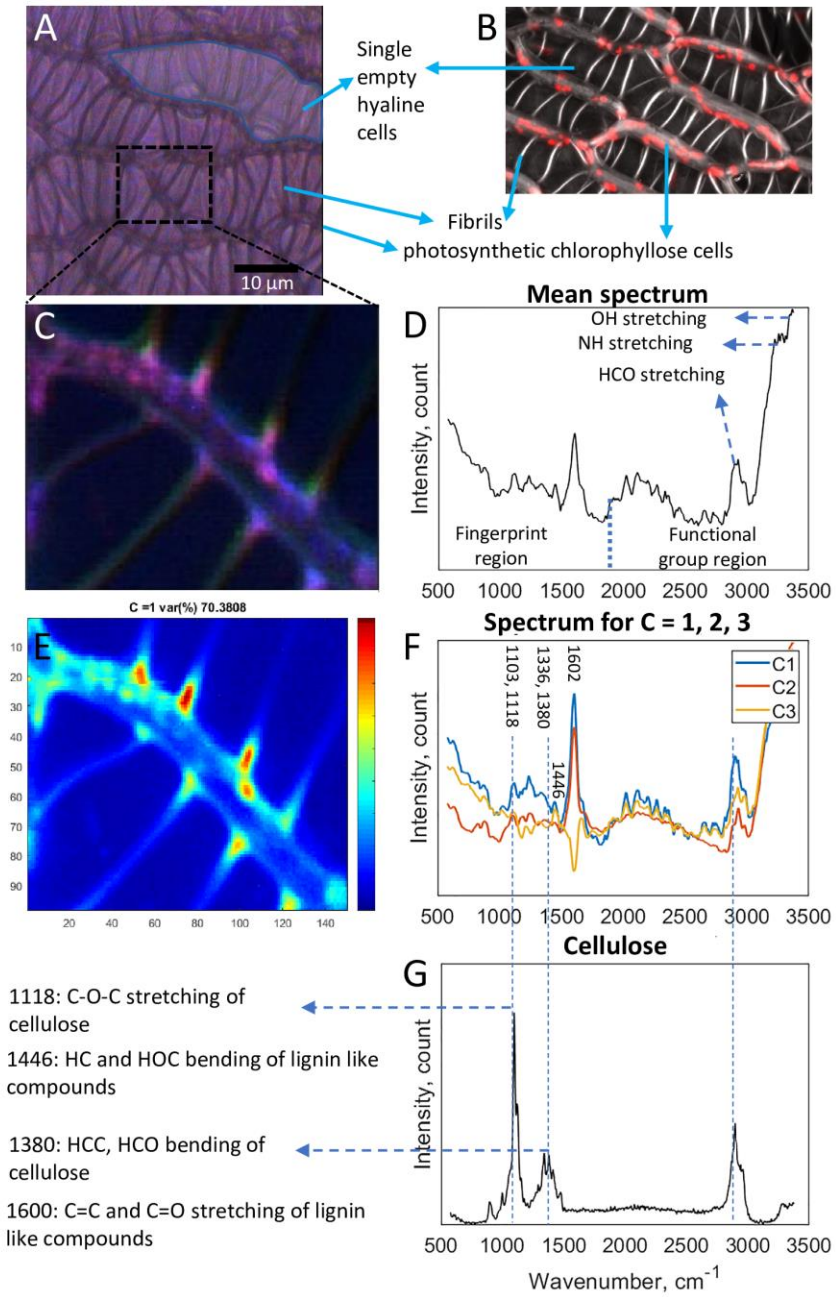

Figure 4: A simplified example of non-destructive spatial identification of cellular components using a hyperspectral Raman image of a *Sphagnum* sp. branch leaf.

Figure 4: A simplified example of non-destructive spatial identification of cellular components using a hyperspectral Raman image of a *Sphagnum* sp. branch leaf.

A) A paradermal image of a *Sphagnum* sp. branch leaf taken by light microscopy. B) A 3D reconstruction of the *Sphagnum* branch leaf stained with calcofluor white to detect cellulose (silver) and autofluorescence of chlorophylls to detect chloroplast, depicting hyaline and photosynthetic chlorophyllose cells. C) Raman hyperspectral image of the rectangular inset in section A, arbitrarily colored. D) Sum of the spectra over the scanned area. E&F) Spatial mapping for the first components (C1) of the MCR-AML Analysis for the Raman spectra (E) and MCR-AML corresponding spectra (F, C1-C3). C1 spectrum shows a high concentration of cell wall components such as cellulose (peaks 1103, 1118, 1380) and lignin-like polymers (peaks 1446, 1600, which spatially corresponds with the cell walls of chlorophyllose cells and the fibrils of hyaline cells. G) Raman spectrum of commercial cellulose used as a reference here. Leaf and cellulose imaged by a WiTec alpha 330; excitation = 523 nm; Lateral resolution = 0.3 µm; spectral resolution = 2.3 cm^{-1}. Terminology for leaf cells adopted from Weston *et al.* (2017); Raman peaks were identified following Socrates and Socrates (2000) and Zhu *et al.* (2018); MCR-AML analysis has been done in Matlab Hypertools toolbox (Amigo *et al.,* 2015).